3. EPR SPECTROSCOPY

3.1. Lectures

L01 ANTIOXIDANTS IN FOODS CHARACTERIZED BY EPR

ANDREJ STAŠKO[a], VLASTA BREZOVÁ[a],
MARTIN POLOVKA[b] and STANISLAV BISKUPIČ[a]
[a]*Department of Physical Chemistry,* [b]*Department of Chemical Technology of Wood, Pulp and Paper, Faculty of Chemical and Food Technology, Slovak University of Technology, Radlinského 9, SK-812 37 Bratislava, Slovak Republic; andrej.stasko@stuba.sk*

Introduction

Many traditional dietary patterns, also across very old cultures analysed from the present scientific point of view, document a rational protection against chronic diseases. Despite world wide different cultural habits and nutrient profiles, there are some common characteristics of healthy dietary patterns, mostly preferred are fruits and vegetables, legumes, whole grains and fish. At the present there is appreciable evidence on the protective role of foods on different cancers and cardiovascular diseases[1].

The initial steps in chronic degenerative diseases including cancer, autoimmune, inflammatory, cardiovascular, neurodegenerative (Alzheimer's, Parkinson's diseases, multiple sclerosis, Down's syndrome) and aging challenges are increasingly associated with the role of radicals, especially of reactive oxygen species (ROS)[2]. Their generation by a sequential one-electron reduction is shown in Fig. 1.

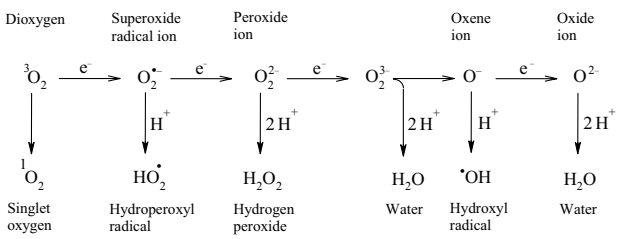

Fig. 1. **Formation of reactive oxygen species (ROS) by the sequential oxygen reduction**

Dioxygen is a bi-radical, fortunately the restriction rules hinder its reactions with the most of organic molecules. However, on energy activation or on electron transfer, its reduction may be initiated up to water producing so ROS intermediates like superoxide anion $O_2^{\bullet-}$, hydroperoxyl HOO$^{\bullet}$ and hydroxyl $^{\bullet}$OH radicals, or also, stable products (H_2O_2) are formed, which may serve as a source of very reactive $^{\bullet}$OH radicals. A controlled ROS production helps the living organisms to manage some of their basic functions, e. g. to kill invading microorganisms, or to realise the photosynthesis. But their uncontrolled production leads to serious damages resulting in numerous diseases.

The living cells evolved sophisticated strategies to keep the concentrations of ROS under a tight control employing various sources of antioxidant systems. Therefore, the study of free radicals and antioxidants promises a new age of health and disease management, starting with the prevention of oxidative reactions in foods, pharmaceutics and cosmetics, up to the role of ROS in chronic and degenerative diseases[3]. The question is raised on the effective tools and methods to characterise the antioxidants and their radical processes.

Our contribution is focused on the characterisation of different antioxidants by means of EPR spectroscopy, which represents an effective technique to study free radicals. Generally, various sources of reactive radicals are used. The most known is Fenton reaction, based on the decomposition of H_2O_2 in the presence of transition metals (Fe^{2+}) generating reactive $^{\bullet}$OH radicals. In our experiments we also used other radical sources such as the decomposition of potassium persulfate forming reactive $SO_4^{\bullet-}$ and consecutively $^{\bullet}$OH radicals, further, the decomposition of azo compound 2,2′-azo-bis(2-methylpropionamidine) hydrochloride (AAPH) generating carbon-centred radicals (consecutively peroxyl radicals in the presence of air). As stable radicals, 2,2-diphenyl-1-picrylhydrazyl (DPPH) and cation radical of 2,2′-azino-bis(3-ethylbenthiazoline-6-sulfonic acid) salt (ABTS$^{\bullet+}$) were also used.

Concerning the antioxidants, there are various definitions of them. In chemistry, antioxidants are substances preventing the oxidation of other molecules, preferentially oxidizing themselves. In medicine and biology, they are able in small quantities to remove toxic metabolites (e. g. ROS) and form non-toxic products. In our investigations, the termination of free radicals in the abovementioned radical sources upon the addition of antioxidants was followed. From the foods beer[4–6], wine[7,8], tea[9] and glucans[10] samples were investigated. As antioxidant models employing DPPH radical source[11] served vitamins C and E, carotenoides, Trolox (water-soluble analogue of Vitamin E) and other. Dealing with relatively reactive and unstable radicals ($K_2S_2O_8$, AAPH sources) EPR spin trapping technique was employed.

Experimental

M a t e r i a l s

5,5-Dimethylpyrroline-N-oxide (DMPO) and Trolox was from Aldrich; α-phenyl-N-tert-butylnitrone (PBN) from Sigma Chemicals, 1,1-diphenyl-2-picrylhydrazyle (DPPH) and ABTS from Fluka; 2,2′-azo-bis(2-methylpropionamidine) hydrochloride (AAPH) from Polysciences, Inc; $K_2S_2O_8$ from Merck and antioxidants from Sigma.

P r o c e d u r e s

Stable free radicals as DPPH and cation radical ABTS$^{\bullet+}$ were used as specified below reporting on DPPH experiment with wine samples. More complex procedure is needed if unstable, reactive radicals are generated, e. g. in the thermal

or photochemical decomposition of $K_2S_2O_8$ or AAPH. The decomposition was carried out directly in the cavity of Bruker EMX EPR spectrometer working in the X-band region using flat cell or a capillary. Due to the high reactivity of radicals formed, their stationary concentrations were very low and therefore monitored by means of spin trapping (DMPO). Spin trap is an EPR-silent compound, which traps the radicals and converts them to the stable adducts well accessible to EPR measurements. The experiments started with reference (solvent, buffer, spin trap without sample) and relatively to this reference the radical concentrations were monitored and evaluated.

More specific information about the experiments applied to follow the antioxidant activity of wine samples, the flavour stability of lager beer or to evaluate the absolute amounts antioxidant equivalents are given below.

In the experiments evaluating the absolute amounts of antioxidant equivalents using $ABTS^{\bullet+}$ or DPPH standards, their concentrations were determined by UV/vis. Then from the time evolution of their EPR spectra upon adding various model antioxidants or also food samples, the $ABTS^{\bullet+}$ or DPPH equivalent points were determined and recalculated into Trolox equivalents (generally, two $ABTS^{\bullet+}$ or DPPH equivalents correspond to the Trolox equivalent).

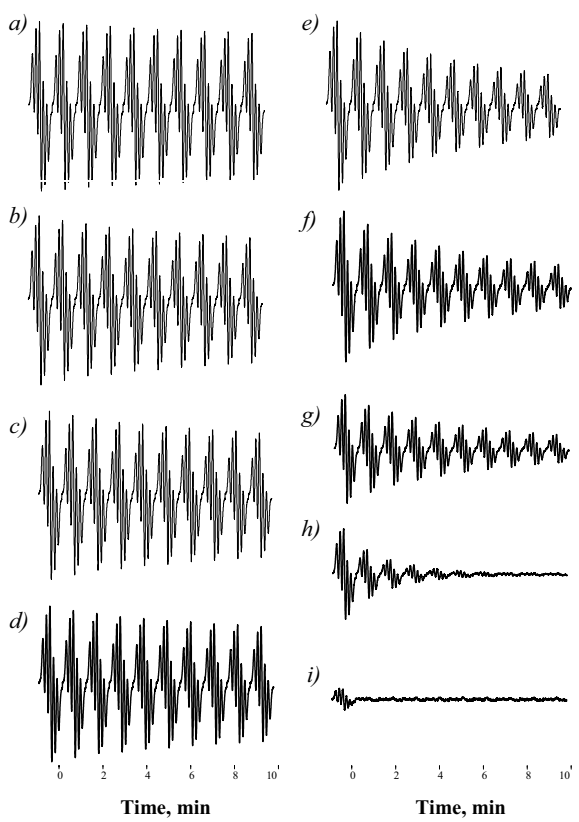

Fig. 2. **The time evolution of EPR spectra from control (a), white (b–c), Tokay (d–g) and red (h–i) wine samples kept at 25 °C for 10 minutes, consisting of 5.10^{-5} M DPPH radicals in solution of ethanol: wine = 40:1**

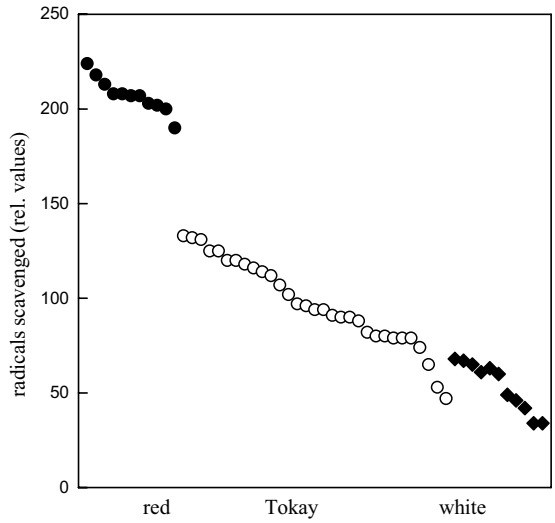

Fig. 3. **Relative amounts of radical scavenged with DPPH radical (a, ●), red, (b, ○) Tokay and (c, ◆) and white wine samples**

Results

Antioxidant activity of wine samples

This series of experiments should illustrate our approach in antioxidant studies. The probe consisting of 5.10^{-5} M DPPH radical solution of ethanol: wine = 40:1 was kept for 10 minutes at 25 °C and the EPR spectra were monitored. The experiments started with a reference (Fig. 2a), where wine was simulated with a 12% aqueous ethanol solution, representing the average content of ethanol in wine sample. It possesses the highest radical concentration. Replacing reference with the white wine samples (b–c), the radical concentration decreased, due to the scavenging of DPPH by wine antioxidants. This is still more expressed in the case of Tokay wines (d–g) and the highest decrease, herewith also the highest scavenging – antioxidant activity showed red wines (h–l). The double integrals from spectra of individual wine samples were evaluated and subtracted from the double integral of EPR spectra of reference sample. In this way, the relative values of the radicals scavenged were obtained. They are quoted for 10 red, 30 Tokay and 10 white wine samples in Fig. 3. As evident, the highest antioxidant activity showed the red wines, followed by the Tokay and the lowest one the white wine samples. A similar relation in the scavenging activities between the red, Tokay and white wines was found using other radical's sources ($K_2S_2O_8$, AAPH and $ABTS^{\bullet+}$).

Beer stability

Basic principles[12,13] in the investigations of lager beer stability shows Fig. 4[4]. The beer probe containing PBN spin trap agent was kept at 60 °C in the cavity of EPR spectrometer in a flat cell or a capillary and the formation of PBN adducts was followed. The induction period in the adduct formation during thermally initiated staling reflects the antioxidants naturally occurring in beer, and its length

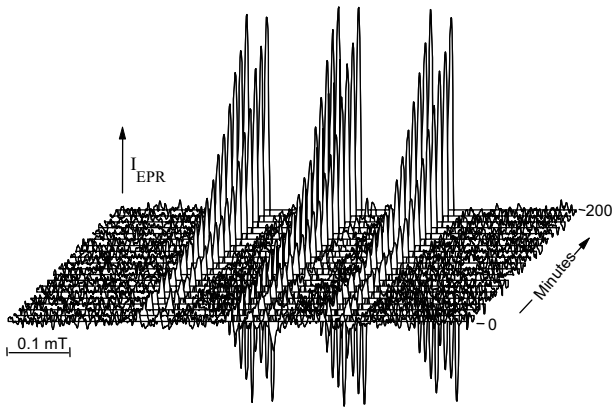

Fig. 4. **The time course of EPR spectra of a lager beer probe followed during 200 minutes at 60 °C in the presence of PBN spin trapping agent**

is taken as a measure for the beer stability (lag time). The addition of ascorbic acid to lager beer samples accelerated the radical process shortening the induction period. On the other hand, Na_2SO_3 added to beer sample prolonged the induction period substantially indicating a higher stabilisation effect. Such an induction period is not evident in the dark and non-alcoholic beers, although the $ABTS^{\bullet+}$ tests confirmed a comparable antioxidant activity of dark and lager beers. A possible explanation for the missing the induction period in the dark and non-alcoholic beers is the presence of more effective antioxidants in the lager beers able rapidly to terminate the initially formed reactive free radicals before their trapping to PBN. Caramel used in the production of dark beers showed relatively high scavenging activity of free radicals and interfered with the antioxidant tests. Non-alcoholic beers indicated, compared to lager und dark beers, a relatively low content of antioxidants in $ABTS^{\bullet+}$ tests.

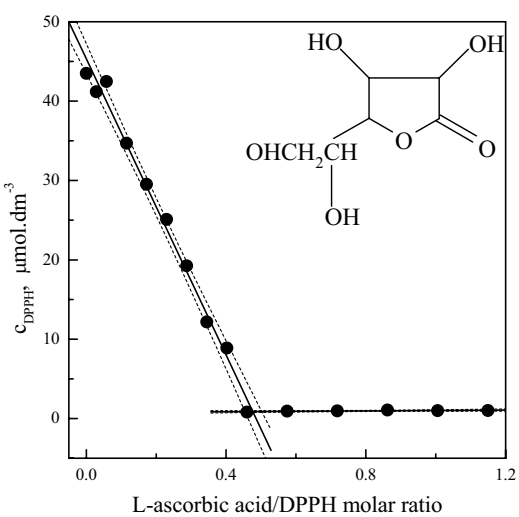

Fig. 5. **The dependence of DPPH concentration upon the increasing ratio of antioxidant – ascorbic acid (HASC) added. The equivalent point is at ratio HASC : DPPH = 1 : 2**

Quantitative antioxidant capacity of the samples

In a series of experiments it is well possible to determine the antioxidant capacity of the samples relatively precise. But to be able to compare the results obtained in various laboratories, an absolute value on the antioxidant capacity is required. There are few standard tests but increasingly as a universal measure, Trolox equivalent is considered in the literature. Trolox is a phenolic antioxidant with a well defined antioxidant stoichiometry (it is oxidised in two-electron steps converting to quinone form). So in the antioxidant tests Trolox is used as a standard. The aim of our presently running investigations is to find a wide scale of molar equivalents using various model antioxidants in their reactions with most frequently employed radical sources in the antioxidant tests. At the present we are investigating DPPH as radical source. An example from such investigations shows Fig. 5. using ascorbic acid (HASC) as antioxidant. On the increasing concentration of HASC added to DPPH solution, the DPPH concentration is decreasing to zero and this point marks the equivalents of DPPH. The most common phenolic antioxidants consume two DPPH molecules. More details on these investigations will be reported in[11].

This work was supported by Science and Technology Assistance Agency under the contract No. APVT-20-005702.

REFERENCES

1. Kris-Etherton P. M., Hecker K. D., Bonanome A., Coval S. M., Binkoski A. E., Hilpert K. F., Griel A. E., Etherton T. D.: Am. J. Med. *113,* 71 (2002).
2. Apel K., Hirt H.: Annu. Rev. Plant Biol. *55,* 373 (2004).
3. Arouma O. I.: Mutation Res. *523,* 9 (2003).
4. Staško A., Rapta P., Malík F.: Monatsschrift für Brauwissenschaft *53,* 4 (2000).
5. Brezová V., Polovka M., Staško A.: Spectrochimica Acta A *58,* 1279 (2002).
6. Staško A., Brezová V., Biskupič S., Šmogrovičová D., Selecký R.: Monatsschrift für Brauwissenschaft, in press. (2005).
7. Staško A., Liptáková M., Malík F., Mišík V.: Appl. Magn. Reson. *22,* 101 (2002).
8. Staško A., Polovka M., Brezová V., Biskupič S., Malík F.: Food Chem., in press (2005).
9. Polovka M., Brezová V., Staško A.: Biophys. Chem. *106,* 39 (2003).
10. Kogan G., Staško A., Bauerová K., Polovka M., Šoltés L., Brezová V., Navarová J., Mihalová D.: Carbohydr. Polym., in press (2005).
11. Staško A., Brezová V.: Spectrochim. Acta A, submitted (2005).
12. Kaneda H., Kano Y., Kamimura M., Osava T., Ramararthnam N., Kawashi S., Kamada K.: J. Food Sci. *55,* 885 (1988).
13. Barr D.: EPR Application Note Bruker Report (1998).

L02 PHOTOCHEMICAL PROCESSES OF CAROTENOIDS INVESTIGATED BY EPR SPECTROSCOPY

VLASTA BREZOVÁ, DANA DVORANOVÁ, MIROSLAVA KLEINOVÁ and MARIÁN VALKO
Department of Physical Chemistry, Faculty of Chemical and Food Technology, Slovak University of Technology, Radlinského 9, SK-812 37 Bratislava, Slovak Republic; vlasta.brezova@stuba.sk

Introduction

Carotenoid pigments (CAR), widely distributed in nature, play important roles in the living organisms, e. g. in light-harvesting antenna systems, electron transfer processes in the photosynthetic reaction centres, retinol (vitamin A) production, in cell protection mechanisms against free radical induced damage[1–3]. The carotenoid structures allow interaction with free radicals by three reaction pathways: *i)* electron transfer, *ii)* hydrogen abstraction, and iii) radical addition. The mechanism and rate of scavenging free radicals is significantly dependent on the CAR structure and radical nature[4]. Carotenoids are excellent visible light absorbers, and the absorption maxima sensitively reflect the number of conjugated double bonds[5]. The unique property of CAR is their ability to quench singlet oxygen ($^1O_2$), produced upon sensitizer (S) photoexcitation in the oxygenated systems (Eqs. 1–4)[6]. The protective function is highly effective, as the chemical quenching rate constant (Eq. 4) is substantially lower comparing to physical quenching rate constant (Eq. 3; $k_{qphys} \sim 10^9$–10^{10} L mol^{-1} s^{-1})[2]. Product analysis for the reaction products of β-carotene with singlet oxygen indicated the formation of the β-carotene-5,8-endoperoxide as the primary oxidation product, and additionally β-ionone, β-apo-14'-carotenal, β-apo-10'-carotenal, β-apo-8'-carotenal were identified[6–8].

$$S \xrightarrow{h\nu} {}^1S^* \xrightarrow{ISC} {}^3S^* \quad (1)$$

$${}^3S^* + {}^3O_2 \xrightarrow{\text{energy transfer}} S + {}^1O_2 \quad (2)$$

$${}^1O_2 + CAR \xrightarrow{\text{physical quenching}} {}^3O_2 + {}^3CAR^* \quad (3)$$

$${}^3CAR^* \rightarrow CAR + \text{heat}$$

$${}^1O_2 + CAR \xrightarrow{\text{chemical quenching}} CARO_2 \quad (4)$$

The decomposition of β-carotene induced by light and oxygen is well known. The reaction mechanism involves consecutive photoisomerization and photooxidation steps resulting in the formation of epoxides, apocarotenoids, and finally low molecular products[5]. The investigations of photodegradation of β-carotene and canthaxanthin at various wavelengths (313 nm, 334 nm, 366 nm, 405 nm, 436 nm) confirmed that the photodegradation quantum yield significantly increases with the decreasing wavelength; in addition the oxygen-dependent and oxygen-independent reaction pathways were suggested for photoexcitation with 366 nm wavelength[9]. Recently, the generation of super oxide anion radicals and singlet oxygen upon irradiation ($\lambda = 350$ nm) of TiO_2 nanoparticles sensitized by carotenoids was demonstrated using EPR spectroscopy[10].

Our study focuses on EPR investigations of reactive radical intermediates and singlet oxygen generated by the irradiation of all-β-*trans*-carotene (trans-β-CAR) in different solvents (dimethyl sulfoxide, ethanol) under argon, air or oxygen atmosphere.

Experimental

All-β-*trans*-carotene (Scholl of Pharmacy, Liverpool UK) was kept in the dark at –18 °C. The *trans*-β-CAR stock solutions for EPR experiments, prepared immediately before measurements, were also saved in the dark. Spin trapping agents, α-(4-pyridyl-1-oxide)-N-*tert*-butylnitrone (POBN, Aldrich) and 5,5-dimethyl-1-pyrroline N-oxide (DMPO, Aldrich) were stored at –18 °C. DMPO was distilled before application and saved under argon. Stable free radical 4-hydroxy-2,2,6,6-tetramethylpiperidine N-oxyl (TEMPOL) and selective singlet oxygen trap 4-hydroxy-2,2,6,6-piperidine (TMP) were purchased from Aldrich. Superoxide dismutase (SOD, 30 000 units, from bovine erythrocytes) from Sigma-Aldrich was used. Dimethyl sulfoxide (DMSO) and ethanol purchased from Merck were used without further purification.

EPR measurements at the X-band were performed with a Bruker EMX EPR spectrometer equipped with a TM-110 (ER 4103 TM) cylindrical cavity. The samples were irradiated at 293 K directly in the EPR spectrometer microwave cavity, and the EPR spectra were recorded in situ. As an irradiation source an HPA 400/30S lamp (400 W, Philips) was used; it is a medium-pressure metal halide lamp with iron and cobalt additives emitting ozone-free radiation mainly between 300 and 400 nm ($\lambda_{max} = 365$ nm). The source radiation was focused to obtain high intensity in the active part of the TM cylindrical resonator. The lamp irradiance in the UVA region of 30 mW cm^{-2} inside the EPR cavity was determined using a Compact radiometer UVPS (UV Process Supply, Inc. USA). A Pyrex glass filter (thickness of 1 mm) was applied to eliminate the radiation wavelengths below 300 nm.

The experimental EPR spectra acquisition and simulation was carried out using WIN EPR and SimFonia standard programs (Bruker). The multicomponent experimental EPR spectra were evaluated as a linear combination of individual EPR spectra simulations by a least-squares minimization procedure with the Scientist Program (MicroMath). The statistical parameters of calculation procedure (R^2, coefficient of determination and correlation) serve for the determination of simulation quality, i. e. harmonization of experimental and simulated spectra. The relative concentration of the individual paramagnetic species was evaluated in the simulation from the contributions of their individual spectra to the experimental spectrum after double integration.

Results and discussion

Fig. 1a illustrates experimental and simulated EPR spectra obtained upon 20 minute exposure ($\lambda > 300$ nm) of argon-saturated DMSO solution of *trans*-β-CAR in the presence of DMPO as the spin trap. The Hamiltonian parameters of the EPR signals obtained by simulation analysis confirmed the generation of $^{\bullet}$DMPO-CR adduct[11], characterized by hyperfine splittings $a_N = 1.458$ mT, $a_H^{\beta} = 2.110$ mT and g-value = 2.0056. The generation of carbon-centred radical species, which is added to DMPO, probably reflects the photoinduced symmetric or asymmetric cleavage of carotene chain under inert atmosphere[12]. The EPR spectrum monitored upon the analogous photoexcitation of *trans*-β-CAR in DMSO aerated solutions (Fig. 1b), represents superposition of five individual EPR signals of radical intermediates added to DMPO: *i)* $^{\bullet}$DMPO-O_2^- characterized by $a_N = 1.282$ mT, $a_H^{\beta} = 1.020$ mT, $a_H^{\gamma} = 0.133$ mT; g = 2.0059; relative concentration 48.3 %, *ii)* $^{\bullet}$DMPO-OCH_3 ($a_N = 1.335$ mT, $a_H^{\beta} = 0.795$ mT, $a_H^{\gamma} = 0.160$ mT; g = 2.0058; 43.2 %), *iii)* $^{\bullet}$DMPO-OR_1 ($a_N = 1.395$ mT, $a_H^{\beta} = 1.140$ mT; g = 2.0057; 5.8 %), *iv)* $^{\bullet}$DMPO-OCR_2 ($a_N = 1.417$ mT, $a_H^{\beta} = 1.720$ mT; g = 2.0057; 1.7 %), *v)* $^{\bullet}$DMPO-CR ($a_N = 1.515$ mT, $a_H^{\beta} = 1.995$ mT; g = 2.0056; 1.0 %).

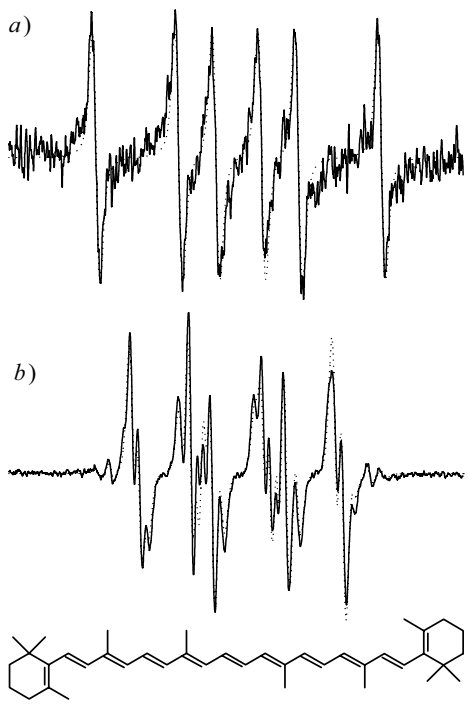

Fig. 1. **Experimental (solid line) and simulated (dotted line) EPR spectra (sweep width 8 mT) monitored upon 20 minutes exposure ($\lambda > 300$ nm) of *trans*-β-CAR in DMSO solvent in the presence of DMPO spin trap: *a)* under argon; *b)* under air. Initial concentrations: c_0(DMPO) = 0.035 mol dm^{-3}, c_0(*trans*-β-CAR) = 2.3 mmol dm^{-3}**
The simulation parameters and spin adducts attribution is discussed in text
The inset represents the structure of all-*trans*-β-carotene

The proposed mechanism of the free radical formation upon irradiation ($\lambda > 300$ nm) of all-trans-β-carotene could be summarized as follows (Eqs. 5–17):

$$\textit{trans}\text{-}\beta\text{-CAR} + h\nu \rightarrow (\textit{trans}\text{-}\beta\text{-CAR})^* \quad (5)$$

$$(\textit{trans}\text{-}\beta\text{-CAR})^* \rightarrow \textit{cis}\text{-}\beta\text{-CAR} \quad (6)$$

$$(\beta\text{-CAR})^* \rightarrow {}^{\bullet}R + {}^{\bullet}R' \quad \text{(symmetric or assymetric chain cleavage)} \quad (7)$$

$$(\beta\text{-CAR})^* + O_2 \rightarrow (\beta\text{-CAR})^{+\bullet} + O_2^{-\bullet} \quad (8)$$

$$(\beta\text{-CAR})^{+\bullet} + O_2 \rightarrow (\beta\text{-CARO}_2)^{+\bullet} \quad (9)$$

$$(\beta\text{-CAR})^{+\bullet} + O_2^{-\bullet} \rightarrow \beta\text{-CARO}_2 \quad (10)$$

$$R^{\bullet} + O_2 \rightarrow ROO^{\bullet} \quad (11)$$

$$ROO^{\bullet} + \beta\text{-CAR} \xrightarrow{\text{electron transfer}} ROO^- + (\beta\text{-CAR})^{+\bullet} \quad (12)$$

$$ROO^{\bullet} + \beta\text{-CAR} \xrightarrow{\text{hydrogen abstraction}} ROOH + \beta\text{-CAR}^{\bullet} \quad (13)$$

$$ROO^{\bullet} + \beta\text{-CAR} \xrightarrow{\text{addition}} (ROO\text{-}\beta\text{-CAR})^{\bullet} \quad (14)$$

$$ROOH, (ROO\text{-}\beta\text{-CAR})^{\bullet}, ROO^- \xrightarrow{h\nu} {}^{\bullet}OR', {}^{\bullet}COR, {}^{\bullet}OH \quad (15)$$

$${}^{\bullet}OH + (CH_3)_2SO + O_2 \rightarrow CH_3(OH)SO + {}^{\bullet}OOCH_3$$

$$2\,{}^{\bullet}OOCH_3 \rightarrow {}^{\bullet}OCH_3 + O_2 \quad (16)$$

$$DMPO + \text{radical intermediates} \rightarrow {}^{\bullet}\text{DMPO-adducts} \quad (17)$$

The generation of carbon- and oxygen-centred spin adducts upon irradiation of *trans*-β-CAR in the oxygenated DMSO solutions were evidenced also using POBN spin trapping agent. The addition of SOD into *trans*-β-CAR solutions causes the significant decrease of $^{\bullet}$DMPO–O_2^- or $^{\bullet}$POBN–O_2^- signal intensities observed during photoexcitation, demonstrating so unambiguously the generation of super oxide anion radical under given experimental conditions.

The application of photochemically stable free radical TEMPOL for the detection of free radical formation (monitoring the decrease in its EPR intensity resulting from the interaction of its >N–O$^{\bullet}$ group with the generated reactive radical species[13]) showed the substantial decrease of TEMPOL concentration upon irradiation of *trans*-β-CAR solutions saturated by argon and air (Fig. 2.).

However, the analogous photochemical experiment carried out in the oxygen-saturated *trans*-β-CAR solutions in the presence TEMPOL revealed the re-oxidation of nitroxide group. The possible explanation of this phenomenon brought the experiments using TMP, exploiting its selective reaction

with $^1O_2$, which resulted in the formation of stable nitroxide free radical TEMPOL[13]. The process of singlet oxygen production upon irradiation of *trans*-β-CAR in DMSO solutions could be explained by the direct energy transfer between photoexcited β-CAR molecules and molecular oxygen, or by the super oxide anion radical termination, as proposed previously by Konovalova et al[10].

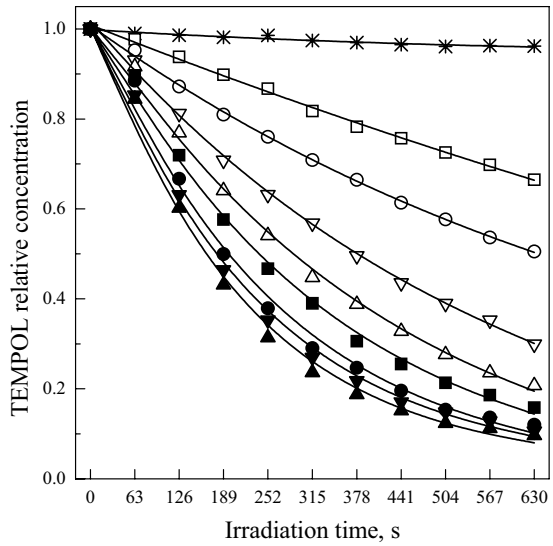

Fig. 2. **Decrease of TEMPOL relative concentration monitored upon continuous irradiation (λ > 300 nm) of *trans*-β-CAR in DMSO solvent in the presence of stable nitroxide radical TEMPOL (c_0(TEMPOL) = 10 μmol dm^{-3}) under argon. Initial concentrations of *trans*-β-CAR (mmol dm^{-3}): ✶ 0; □ 0.29; ○ 0.58; ▽ 0.87; △ 1.17; ■ 1.46; ● 1.75; ▼ 2.04; ▲ 2.33**

We thank Slovak Grant Agency for the financial support (Projects VEGA/1/0053/03 and 1/2450/05).

REFERENCES

1. Krinsky N. I.: Pure & Appl. Chem. *66*, 1003 (1994).
2. Martin H. D., Ruck C., Schmidt M., Sell S., Beutner S., Mayer B., Walsh R.: Pure & Appl. Chem. *71,* 2253 (1999).
3. Young A. J., Lowe G. M.: Arch. Biochem. Biophys. *385,* 20 (2001).
4. El-Agamey A., Lowe G. M., McGarvey D. J., Mortensen A., Phillips D., Truscott T. G., Young A. J.: Arch. Biochem. Biophys. *430,* 37 (2004).
5. Rodriguez-Amaya D. B.: *A Guide to Carotenoid Analysis in Foods*. ILSI Press, International Life Sciences Institute, Washington, 2001.
6. Montenegro M. A., Nazareno M. A., Durantini E. N., Borsarelli C. D.: Photochem. Photobiol. *75,* 353 (2002).
7. Stratton S. P., Schaefer W. H., Liebler D. C.: Chem. Res. Toxicol. *6,* 542 (1993).
8. Gao Y., Kispert L. D.: J. Phys. Chem. B *107,* 5333 (2003).
9. Nielsen B. R., Mortensen A., Jřrgensen K., Skibsted L. H.: J. Agric. Food Chem. *44,* 2106 (1996).
10. Konovalova T. A., Lawrence J., Kispert L. D.: J. Photochem. Photobiol. A: Chem. *162,* 1 (2004).
11. Li A. S. W., Cummings K. B., Roethling H. P., Buettner G. R., Chignell C. F.: J. Magn. Reson. *79,* 140 (1988).
12. Caris-Veyrat C., Amiot M.-J., Ramasseul R., Marchon J.-C.: New J. Chem. *25,* 203 (2001).
13. Brezová V., Gabčová S., Dvoranová D., Staško A.: J. Photochem. Photobiol. B: Biol. in press (2005).

L03 OREGANO INVESTIGATED BY MEANS OF EPR SPECTROSCOPY

MARTIN POLOVKA[a], VLASTA BREZOVÁ[b], ANDREJ STAŠKO[b], MILAN SUHAJ[c] and JANA RÁCZOVÁ[c]
[a]Department of Chemical Technology of Wood, Pulp and Paper, [b]Department of Physical Chemistry, Faculty of Chemical and Food Technology, Slovak University of Technology in Bratislava, Radlinského 9, SK-812 37 Bratislava, Slovak Republic. [c]Food Research Institute, Priemyselná 4, P. O. Box 25, SK-824 75 Bratislava, martin.polovka@stuba.sk

Introduction

Oregano (Origanum vulgare, L.) is aromatic spice frequently used all over the world. It contains numerous amount of different antioxidants; derivatives of phenolic acids, flavonoids, tocopherols, rosmarinic acid, carvacrol, and thymol are the most significant from them[1,2]. According to phytochemical database[3], number of different antioxidants in this spice reaches up to thirty four.

During its preparation, processing and storage, it frequently undergoes microbial contamination. The γ-irradiation treatment of food and plant products is nowadays accepted as a standard and safe sterilization technique, which lowers the risk of microbiological contaminations and prolongs the durability of products[4]. The protection of customer requires unambiguous determination as to whether nutrition products have been exposed to γ-irradiation even for long periods after the radiation process[5–7]. Consequently the European Committee for Standardization (CEN) in EN 1787:2000 proposed an EPR method for detection of food containing irradiated cellulose and later standardized four additional methods for the detection of irradiated food, (i. e. EN 13708:2001, EN 13751:2002, EN 13783:2001 and EN 13784:2001).

EPR spectroscopy is unique technique for the detection of paramagnetic species which are formed during the γ-radiation process but its application is limited by the lifetime of radiolytically produced free radicals[6–9]. The main aim of the presented investigation was the study of radical species produced upon γ-radiation treatment of oregano samples using EPR spectroscopy.

Experimental

Sample characterisation. Commercially available oregano from Cambidi – Izmir – Turkey, was used. The spice

samples were irradiated using ^{60}Co source at doses of 2.5, 5, 10, and 30 kGy according to commercial practices at Artim, Ltd., Prague, Czech Republic on June 10, 2004. Mean dry matter content of oregano was between 90.1–90.6 % (w/w). All samples were stored in closed bags in the dark at 6 °C and at a relative humidity of 60 %.

EPR measurements. Oregano (100 mg) was placed in thin-wall quartz EPR tubes (internal diameter of 3 mm, length of 150 mm, and wall thickness about 0.1 mm) to produce cylindrical samples with identical dimensions (sample column height 5.2 ± 0.2 cm). The sample was then inserted into a standard TE_{102} (ER 4102 ST) rectangular cavity of an EMX X-band EPR spectrometer (Bruker, Germany) and the EPR spectrum was recorded at various temperatures. Temperature control was achieved using a Bruker temperature control unit ER 4111 VT. The careful filling procedure of EPR cells resulted in good reproducibility between samples with a standard deviation in the relative EPR intensity of ±5 % for five independent measurements. The EPR spectrometer settings were as follows: microwave frequency, 9.45 GHz; microwave power, 0.63–31.73 mW; center field, 335.4 mT; sweep width, 20–500 mT; gain, 5.10^5; modulation amplitude, 0.05 mT; modulation frequency, 100 kHz; scan, 84 s; time constant, 40.96 ms, number of scans, 5; temperature, 298–373 K. The g-values were determined with uncertainty of ±0.0005 by simultaneous measurement of a reference sample containing DPPH fixed on EPR cell. The EPR instruments settings for quantitative evaluation were examined by DPPH standard.

The experimental EPR spectra processing and simulation was carried out using *WIN EPR* and *SimFonia* programs (Bruker). The integral intensities of the EPR signals were obtained by double integration of the spectrum. The multi-component experimental EPR spectra were evaluated as a linear combination of individual EPR spectra simulations using a least-squares minimization procedure with the *Scientist Program* (MicroMath).

Statistical analysis. The statistical parameters of the calculation procedure (R-squared, coefficient of determination and correlation) serve as a determination of the simulation quality, i. e. correlation of the experimental and simulated spectra. The relative concentration of the individual paramagnetic species was evaluated from the contributions of the individual simulations to experimental spectrum after double integration.

Results and discussion

Firstly, the EPR spectra of all investigated oregano samples were measured using magnetic field width of 500 mT. Obtained spectra clearly demonstrate a broad singlet line with unresolved hyperfine splittings (Fig. 1a.). As oregano is of plant origin, this line was attributed to Mn^{2+} ions, in accordance with previously published data[10,11] upon which is superimposed a sharp EPR signal, whose intensity is strongly dependent on absorbed γ-radiation dose. Detail of above mentioned sharp EPR spectra, measured one week after irradiation treatment, is better visible in Fig. 1b, where the magnetic field sweep width was lower to 20 mT.

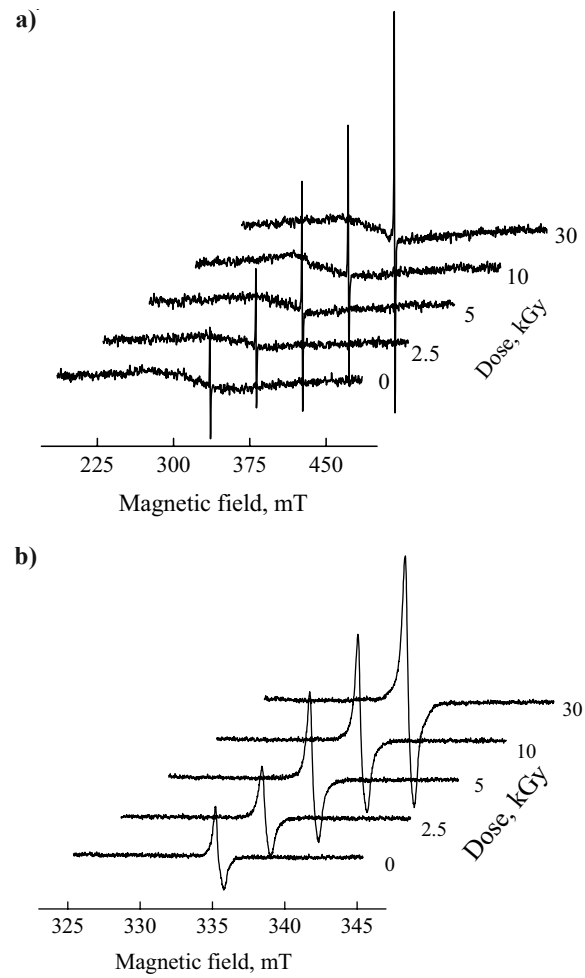

Fig. 1. **X-band EPR spectra of reference (non-irradiatred) oregano sample (0) and oregano samples after γ-radiation treatment at various doses (2.5–30), measured at 298 K using microwave power 0.633 mW and magnetic field sweep width: *a)* 500 mT; *b)* 20 mT**

Fig. 2. shows the dependence of total EPR intensity of oregano samples on absorbed dose of gamma radiation, evaluated for EPR spectra measured at 298 K using 0.633 mW microwave power one week, 5 and 10 months after γ-radiation treatment, respectively. As it is shown, the stability of gamma radiation induced radicals is dependent on storage time.

The total EPR intensity of γ-radiation induced radical species is significantly related to the γ-radiation dose and can be well fitted using the model of saturation curve.

The experimental spectra of non-irradiated (reference) sample and sample treated with a γ-radiation dose of 30 kGy are shown in the inset of Fig. 2. The spectrum of reference sample was simulated as sharp singlet line characterized by

$g_{\perp}$ = 2.0044, $g_{||}$ = 2.0010, and ΔB_{pp} = 0.285 mT which can be attributed to semiquinone radicals produced by the oxidation of polyphenolic compounds present in plants[10–12]. The application of gamma radiation on oregano samples lead to the formation of three additional EPR signals – i) anisotropic triplet ($A_{\perp}$ = 0.85 mT, $A_{||}$ = 0.7 mT; $g_{\perp} = g_{||}$ = 2.0061; ΔB_{pp} = 0.67 mT) attributed to carbohydrates radical structures[13,14]; ii) anisotropic triplet ($A_{\perp}$ = 3.0 mT, $A_{||}$ = 1.8 mT; $g_{\perp}$ = 2.0060, $g_{||}$ = 2.0050; ΔB_{pp} = 1.2 mT previously attributed to "cellulosic" radical species[8,9,15,16] and iii) anisotropic singlet ($g_{\perp}$ = 2.0073, $g_{||}$ = 2,0034; ΔB_{pp} = 0.4 mT).

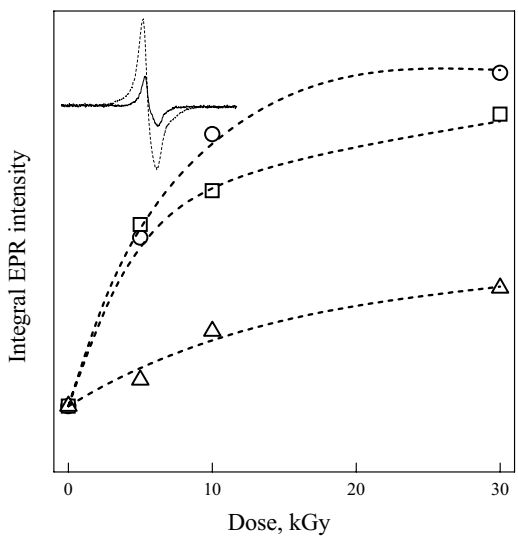

Fig. 2. **The dependence of integral EPR intensity of oregano samples on γ-radiation dose evaluated for EPR spectra measured at 298 K using 0.633 mW microwave power one week (○), 5 months (□) and 10 months (△) after irradiation**
Inset represents the experimental EPR spectra of reference, non-irradiated sample (–) and oregano sample irradiated at dose 30 kGy (···), respectively. Magnetic field width 8 mT. (EPR spectra were recorded 1 week after γ-radiation treatment)

However, the EPR signal of cellulosic radical species, which the European Committee for Standardization in EN 1787:2000 declared as a marker of gamma irradiation of natural cellulose-containing materials is minimal[17].

The stability of radiation-induced radicals is strongly temperature-dependent. As depicted at Fig. 3., the EPR spectra of the reference sample showed only negligible changes upon increasing temperature from 298 K to 353 K. On the other hand, the behavior of irradiated samples under increasing temperature is quite different. The rising of temperature from 298 K to 373 K caused a significant and irreversible decrease of γ-radiation induced EPR signals. However, increasing the temperature to 373 K caused the increase of EPR signal intensity, probably due to the thermal decomposition of sample and formation of new, thermally induced radicals, as it was previously described by Franco et al[18].

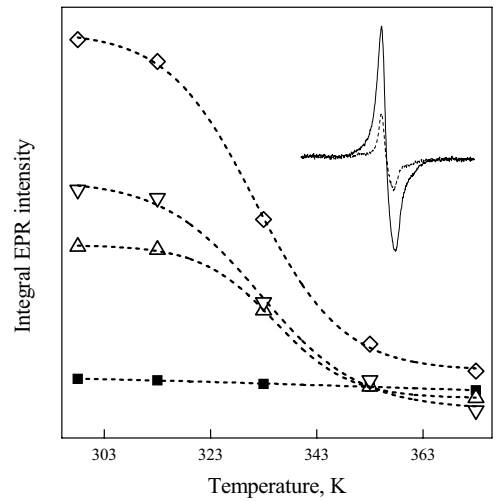

Fig. 3. **The dependence of integral intensity of EPR spectra of oregano samples on temperature measured at 0.633 mW microwave power one week after γ-irradiation for reference (non-irradiated) sample (■), and sample with adsorbed dose: 5 kGy (△), 10 kGy(▽), 30 kGy (◇)**
Inset represents the experimental EPR spectra of sample irradiated at dose 30 kGy, measured at 298 K (–) and at 373 K(···), respectively. Magnetic field width 8 mT. (EPR spectra were recorded 1 week after γ-radiation treatment)

The study of thermal stability of EPR signal can be useful in prediction of previous irradiation treatment of cellulose-containing sample of natural origin. The exact mathematical evaluation of measured spectra could determine the rate of thermal termination for each detected type of radical structures.

We thank Slovak Grant Agency (Project VEGA/1/0053/03) for its financial support.

REFERENCES

1. Pizzale L., Bortolomeazzi R., Vichi S., Conte L. S.: J. Sci. Food Agric. *82,* 1645 (2002).
2. Peter K. V.: *Handbook of herbs and spices.* CRC Press, Woodhead Publishing Ltd., Cambridge 2000.
3. USDA, ARS, National Genetic Resources Program. Phytochemical and Ethnobotanical Databases. http://www.ars-grin.gov/duke/ (2003).
4. Oh K. N., Lee S. Y., Lee H. J., Kim K. E., Yang J. S.: Food Control *14,* 489 (2003).
5. Delincée H.: Radiat. Phys. Chem. *63,* 455 (2002).
6. Raffi J., Yordanov N. D., Chabane S., Douifi L., Gancheva V., Ivanova S.: Spectrochim. Acta A *56*, 409 (2000).
7. Desrosiers M. F.: Appl. Radiat. Isot. *47*, 1621 (1996).
8. Yordanov N. D., Gancheva V.: Appl. Radiat. Isot. *52*, 1958 (2000).
9. Yordanov N. D., Gancheva V., Radicheva M., Hristova B., Guelev M., Penchev P.: Spectrochim. Acta A *54*, 2413 (1998).

10. Morsy M. A.: Spectrosc.-Int. J. *16*, 371 (2002).
11. Polovka M., Brezová V., Staško A.: Biophys. Chem. *106*, 39 (2003).
12. Jezierski A., Czechowski F., Jerzykiewicz M., Golonka I., Drozd J., Bylinska E., Chen Y., Seaward, M. R. D.: Spectrochim. Acta A *58*, 1293 (2002).
13. Korkmaz M., Polat M.: Radiat. Phys. Chem. *62*, 411 (2001).
14. Vanhaelewyn G., Sadlo J., Callens F., Mondelaers W., De Frenne D., Matthys P.: Appl. Radiat. Isot. *52*, 1221 (2000).
15. Bayram G., Delincée, H.: Food Control *15*, 81 (2004).
16. Kispéter J., Bajúsz-Kabók K., Fekete M., Szabó G., Fodor E., Páli T.: Rad. Phys. Chem. *68*, 893 (2003).
17. European Standard EN 1787: Determination of irradiated food containing cellulose: Method by ESR Spectroscopy. (European Committee for Standardization, rue de Stassart 36, B-1050 Brussels, Belgium 2000).
18. Franco R. W. A., Neto L. M., Kato M. S. A, Furlan G. R., Walder J. M. M., Colnago L. A.: Int. J. Food Sci. Tech. *39*, 395 (2004).

L04 EPR APPLICATION IN MEDICINE AND BIOLOGY

PAVEL STOPKA, JANA KŘÍŽOVÁ
and EVA KÁFUŇKOVÁ
Institute of Inorganic Chemistry, Academy of Sciences of The Czech Republic, Group of Bioinorganic Chemistry, 25068 Rez 1001, Czech Republic, stopka@iic.cas.cz

Introduction

Application of the EPR method in biological investigations is associated with studies of paramagnetic centers of two basic types – free radicals and transit valency metal ions, for example, in different metalloenzymes, such as hemoglobin. It was the investigation of the structure of radicals of more or less complex biologically important molecules that prompted one of the first applications of EPR in biology. Investigation of free radicals in biological systems is associated with a difficulty arising from the low concentration of free radicals in cells. Radical concentration in normally metabolizing cells is, according to different sources, about 10^{-8} to 10^{-10} M, while modern radio spectrometers only allow measuring radical concentrations of 10^{-6} to 10^{-7} M. Concentration of free radicals can be increased by increasing their formation rate due to irradiation (UV- or ionizing radiation) or their stabilization at low temperature. The detection of oxygen-generated active radicals is extremely important in biology and it became possible due to the introduction of the method of spin traps. By their chemical nature, spin traps belong to two basic classes – nitrons and nitroso compounds. Well-known examples are C-phenyl-N-tert-butyl nitron (PBN) and 5,5-Dimethyl--pyrroline-N-Oxide (DMPO). Presently, there are data banks containing parameters of the EPR spectra of spin adducts, which allow precise identification and determination of free radical types based on the EPR spectra of spin adducts. Basic information about oxygen reactions in biology, free radicals, antioxidants, spin traps, nitroxides, many related diseases, etc. is described[1]. It is interesting that oxygen molecule is paramagnetic itself. As a result it can interact with nitroxide and make its spectrum broader. This and similar processes are the basis of biological oxymetry, which is possible in vivo. Availability of advanced instrumentation makes it possible to register three dimensional images of biological tissue and to characterize changes of transport and distribution of oxygen in liver, brain and other organ of laboratory animals as a result of different pathology, drug treatment and surgery.

Experimental Part

EPR spectra were recorded on Elexsys E-540 spectrometer (Bruker, Rheinstetten, Germany); magnetic field was measured on a 1H NMR magnetometer, and microwave frequency on a frequency counter The following conditions were used while recording the spectra: microwave power 20 mW, modulation amplitude 0.02 mT, attenuation 20 dB, time constant 0.5 s, scan speed 0.3 mT min^{-1}, calibration standard $Cr3^{+}$/MgO and room temperature. The software used for spectra recording, handling and evaluation was Bruker and WINEPR (Bruker, Germany). 5,5-Dimethyl-1-pyrroline-N-oxide (DMPO) was used as a radical trapping agent.

Results and discussion

There are many EPR applications *in biology* (human, animals, plants) and ***human and veterinary medicine*** (research, diagnostics, therapy). We enumerate our original results only.

M e d i c i n e

a) Direct measurement of free radicals in the brain cortex and the blood serum[2] after nociceptive stimulation in rats: The concentrations of ROS were measured in samples of the sensorimotor brain cortex and the rat blood. Melatonin increased both the hydroxyl and nitroxide radicals. The estimation of ROS can be used as a tool for detecting metabolic changes and the consequences of different environmental influences, in our case the inf luence of nociception and melatonin.

b) Free radicals after painful stimulation are influenced[3] by antioxidants and analgesics: Painful stimulation increased lipoperoxidation which persisted for up to 15 days after it had been discontinued. A simultaneous injection of antioxidants decreased the level of TBARS, SOD and GSHPx: however, antioxidants applied one week prior to the painful stimulation were ineffective. A simultaneous injection of analgesics reduced stress-induced analgesia caused by the nociceptive stimulation, but did not affect lipoperoxidation. A combination of antioxidants with analgesics normalized both the oxidative stress and functional indicators. These results sug-

gest that the administration of antioxidants in pain treatment maybe employed to decrease the doses of analgesics and to prevent the negative impact of reactive oxygen species on nociception.

c) Influence of exogenous melatonin[4] to the free radicals metabolism and pain sensation in rat: Melatonin has been shown to play a role in antioxidative defense. We therefore studied its effect on oxidative damage to the rat cerebral cortex evoked by painful stimulation and immobilization--induced stress. Moreover, the effect of melatonin on chronic pain perception was examined. Rats were injected with either a high dose of melatonin or a vehicle for five days and were subjected to painful stimulation or immobilization stress 30 min. after the treatment. To determine the degree of oxidative stress, the level of free radicals, thiobarbituric acid reactive substances (TBARS) as indicators of lipid peroxidation and glutathione peroxidase (GSHPx) were estimated in somatosensory cortex. Pain perception was measured by the tail-flick and plantar test. Melatonin reduced the level of TBARS previously increased by painful stimulation. Melatonin also exhibited a slight analgesic effect in those animals exposed to painful stimulation but its role in free radical scavenging did not contribute to this effect.

d) Quinolinic Acid-Fe (II) complexes: Slow Autoxidation[5], but enhanced hydroxyl radical production in the Fenton reaction: Quinolinate is a neurotoxic tryptophan metabolite produced mainly by immune-activated macrophages. It is implicated in the pathogenesis of several brain disorders including HIV-associated dementia. The present observations suggest that Quin-Fe (II) complexes display significant pro-oxidant characteristics that could have implications for Quin neurotoxicity.

e) The role of CYP2E1 and 2B1 in metabolic activation[6] of benzene derivatives: oxidation of benzene to covalently binding metabolites was catalyzed by CYP2E1 and 2E1 more effectively than the formation of water-soluble metabolites. Cytochromes P450 in benzene metabolism[7] and involvement of their metabolites and reactive oxygen species in toxicity: cytochromeP450 (CYP) 2E1 was the most efficient CYP enzyme that oxidized benzene to soluble and covalently bound metabolites in rat and human liver microsomes.

f) Influnce of dietary fish oil on the generation of free radicals[9] during reperfusion of isolated rat heart: We investigated, in hereditary hypertriglyceridemic (HTG) rats fed a high-sucrose diet, the effect of fish oil on generation of free radicals (FR) in the isolated heart during post ischemic reperfusion by means of EPR. In the hearts, we identified[10] three different signals of FR: ubisemiquinone ($g = 2.0045$) and iron-sulphur centers ($g = 2.025$ and 1.94), probably associated with mitochondrial respiration. FR contents before ischemia were identical in all three experimental groups. The changes may be associated with increased content of N-3 fatty acids (FA) in myocardial phospholipids.

g) We studied the decolorization of organic natural dyes[11] and we have found the possibility to use hydroxyl radicals for the decolorization and reactions of amino acids[12].

Hair: We studied EPR spectra of melanin in human hair and we have found[13–15] the relation of EPR spectra and some diseases.

B i o l o g y :

a) Zoology

We studied the generation of ROS and RNS in digestive tract of mosquito Anopheles.

b) Botany

Cyanobacteria: We studied content of free radicals (Oxygen radicals), and their photochemical generation and interactions).

Plants: we studied generation of free radicals during their photochemical and pollen interactions.

Plants in vivo: We studied the changes of free radical concentration in plants under chemical stress. (Higher plants, in vivo).

Wooden fungi: The different types of free radicals have been found. (Free radicals and transition metal complexes).

Humic and fulvic acid complexes: We have found sorption of toxic metals, and photochemical degradation of soil humates.

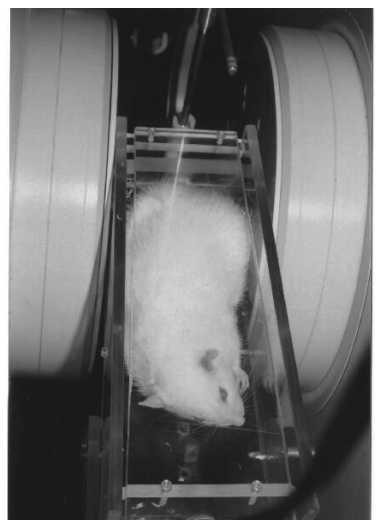

Fig. 1. **Arrangement for EPR study of rats "in vivo"**

REFERENCES

1. Halliwell B., Gutteridge J. M. C. *Free radicals in Biology and Medicine,* 3 ed., Oxford University Press, 2000, and Prof Nikolai Kocherginsky, Unpublished information.
2. Rokyta R., Stopka P., Holeček V., Křikava K: Neuroendocrinology *25*, 252 (2004).
3. Rokyta R., Holeček V., Pekárková I., Krejčová J., Racek J., Trefil L., Yamamotová A.: Neuroendocrinology Letters *24*, 304 (2003).
4. Pekárková I., Parara S., Holeček V., Stopka P., Trefil L., Racek J., Rokyta, R.: Physiological Reserch *50*, 595 (2001).

5. Pláteník J., Stopka P., Vejražka M., Štípek, S.: Free Radicals Research *34*, 445 (2001).
6. Gut I., Nedelcheva V., Soucek P., Stopka P., Vodička P., Gelboin H. V., Ingelman-Sunberg M.: Arch. Toxicol. *71*, 45 (1996).
7. Gut I., Nedelcheva V., Soucek P., Stopka P., Tichavská B.: Environ. Health Perspect *104*, 1211 (1966).
8. Souček P., Gut I., Stopka, P.: Chemico-Biological Interactions *126*, 45 (2000).
9. Vavřínková H., Tutterová M., Stopka P.: Int. Soc. for Heart Research, 15. European Section Meeting, Copenhagen, Denmark, (1994).
10. Vavřínková H., Tutterová M., Stopka P., Divišová J., Kazdová L., Drahota, Z.: Physiological Research *50*, 481 (2001).
11. Verma P., Shah V., Baldrian P., Gabriel J., Stopka P., Trnka T., Nerud, F.: Chemosphere, 54, 291 (2004), and Shah V., Verma P., Stopka P., Gabriel J., Baldrian P., Nerud, F.: Applied Catalysis B: Environmental *46*, 287 (2003).
12. Švorčík V., Hnatowicz V., Stopka P., Bačáková L., Heitz J., Ochsner R.,Ryssel, H.: Radiation Physics and Chemistry *60*, 89 (2001).
13. Stopka P., Křížová J., Navrátilová E., Hálová J.: Klin. Biochem. Metab. *10*, 262 (2002).
14. Stopka P., Havlíčková M., Křížová J., Arenberger P., Votruba M.: Klin. Biochem. Metab. *12*, 196 (2004).
15. Havlíčková M., Stopka P., Křížová J., Arenberger P., Votruba M.: Klin. Biochem. Metab., in press.

L05 EPR STUDY OF RADICAL REACTIONS OF SOME COUMARIN DERIVATIVES

RENATA SUPERATOVÁ[a], LADISLAV OMELKA[a] and JAN SVĚTLÍK[b]
[a]*Institute of Physical and Applied Chemistry, Faculty of Chemistry, Brno University of Technology, Purkyňova 118, 612 00 Brno, superatova@fch.vutbr.cz*
[b]*Department of Pharmaceutical Analysis and Nuclear Pharmacy, Faculty of Pharmacy, Odbojarov 10, SK-835 32 Bratislava*

Introduction

Strategy based upon free-radical reactions has become a powerful tool for the construction of various types of carbocyclic, heterocyclic compounds and complex target molecules. Radical chemistry is now playing a great role in the organic synthesis due to several advantages such as mild reaction conditions, high functional group tolerance, high stereoselectivities and the possibility of cascade processes. Recently we have reported a preparative route to substituted benzopyrano [4,3–b] pyridines[1]. The cyclisation proceeds through 3-acetoacetylcoumarin which appears to be a valuable intermediate in heterocyclic synthesis. Methylene group in this diketone could be prone to homolysis of the active C-H bond to form corresponding alpha-acyl radical. Generation, detection and study of the alpha-keto radicals from this precursor and related compounds can open a way for further synthetic utility of these coumarins.

Experimental

0.3 ml of 0.1 M benzene solution of substituted coumarin was mixed with identical volume of 0,1 M solution of spin trap in EPR tube. To this solution 10 mg of PbO_2 was added. Subsequently nitrogen was bubbled through the suspension formed for 30 sec. Using this procedure the effective contact of solid phase with solution was achieved. On the other side, the bubbling with inert gas enables to obtain optimal conditions for the registration of high quality EPR spectra. EPR spectra were measured at laboratory temperature using EPR spectrometer SpectraNova. The simulation of experimental EPR spectra was performed using the simulation programme Symphonia.

Results and discussion

Radical reactions of substituted coumarin derivatives **1–4** and these of related structures **5** and **6** were investigated using EPR spectroscopy.

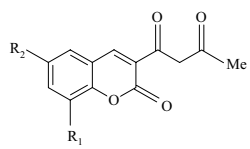

1
1a R_1 = OMe, R_2 = H
1b R_2 = Br, R_1 = H

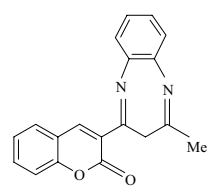

2

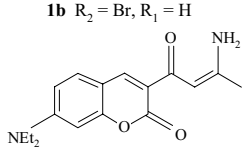

3

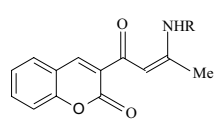

4
4a R = $CH_2CH(Me)_2$
4b R = *p*-BrC_6H_4
4c R = CH_2-C_6H_5

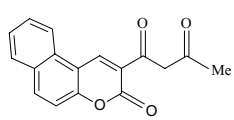

5

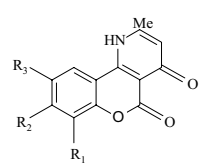

6
6a R_2 = NEt_2, R_1 = R_3 = H
6b R_1 = R_3 = Cl, R_2 = H
6c R_3 = Br, R_1 = R_2 = H
6d R_3 = NO_2, R_1 = R_2 = H

Radical generation from acetoacetylcoumarins **1a** and **1b** was studied on the surface of PbO_2 in benzene solution. In the absence of spin trap no EPR signal was observed. However, performing the reaction in the presence of spin trap, high

concentration of radical adduct was obtained. In the presence of nitrosobenzene EPR spectrum, shown in Fig. 1., was registered. Taking into account determined EPR parameters
(**1a**: 1 . a_N(NO) = 1.018 mT, 1 . a_H = 0.467 mT,
3 . a_H(*o, p*) = 0.258 mT, 2 . a_H(*m*) = 0.086 mT;
1b: 1 . a_N(NO) = 1.030 mT, 1 . a_H = 0.460 mT,
3 . a_H(*o, p*) = 0.270 mT, 2 . a_H(*m*) = 0.090 mT)
it is evident that the radical added contains one hydrogen atom in the α-position. With respect to the structure of the investigated coumarins, this fact can be interpreted as a result of hydrogen abstraction from the methylene group in the 3-acetoacetyl substituent, where C-radicals **7a, 7b** are formed. It means that the mechanism of hydrogen abstraction on the surface of PbO_2 and consecutive addition to spin trap (radical adducts **8a, 8b**) is as follows (Scheme 1). Nitroxyl radicals similar to **8a, 8b** were reported to be formed also by direct reaction between nitroso spin traps (CF_3NO, nitrosobenzene) and some 1,3-diketones.[2,3] However, this reaction route was not confirmed with 3-acetoacetyl coumarin derivatives.

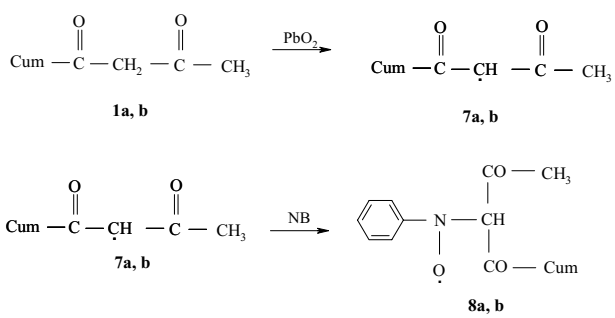

Sheme 1

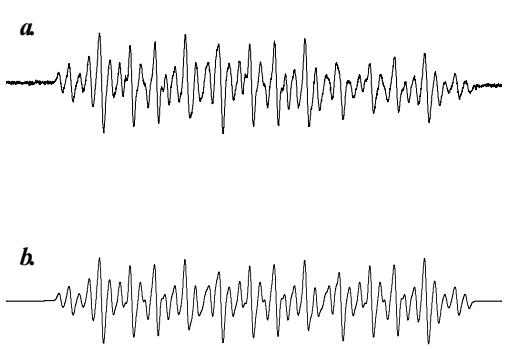

Fig. 1. **Experimental (a) and simulated (b) EPR spektrum of radical adduct** 8b

This experimental result also points out that radical adduct is formed only from the keto form of acetoacetyl substituent, although keto-enol tautomerism is known to occur in this case[1]. Behavior of **1a** on the surface of PbO_2 was also studied in the presence of other spin traps. In all adducts the additional splitting from one hydrogen atom was observed (nitrosodurene: 1 . a_N(NO) = 1.21 mT, 1 . a_H = 0.694mT; 2-methyl-2-nitrosopropane: 1 . a_N(NO) = 1.325 mT, 1 . a_H = 0.437 mT; 2.4,6-tritertbutylnitrosobenzene: 1 . a_N(NO) = 1.214 mT, 1 . a_H = 0.725 mT; nitrosotoluene: 1 . a_N(NO) = 1.109 mT, 2 . a_H(*o, p*) = 0.18 mT, 3 . a_H(CH_3) = 0.18 mT, 2 . a_H(*m*) = 0.08 mT, 1 . a_H = 0.395 mT).
Experimental and simulated EPR spectrum of radical adduct with nitrosotoluene is outlined in Fig. 2. EPR spectrum of radical adduct, where (besides the splittings derived from spin trap atoms) additional splitting from one hydrogen atom is involved, was also observed with the compound **2** (2 . a_N(NO) = 1,03 mT, 3 . a_H = 0,256 mT, 2 . a_H = 0,09 mT, 1 . a_H = 0,511 mT). Moreover, this spectrum does not substantially differ from that of radical adduct derived from structure **3**. This finding suggests that also in compound **3** the tautomeric form dominates, where the hydrogen atom from aminogroup is transferred to the methine moiety (amino--imino tautomerism).

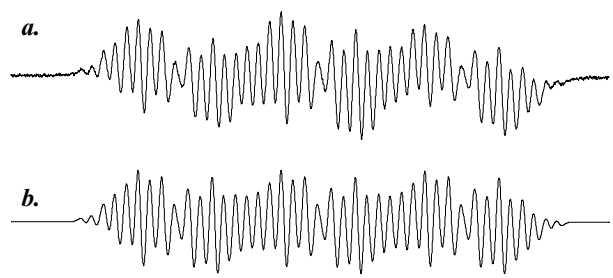

Fig. 2. **Experimental (a) and simulated (b) EPR spectrum of radical adduct** 7b **with nitrosotoluene**

By the study of the behavior of substituted enaminocoumarins **4** on the surface of PbO_2 no radical intermediates were observed in the abssence of spin trap. The presence of secondary NH– group in the side chain, however, suggests that besides possible H-abstraction in this position (radical

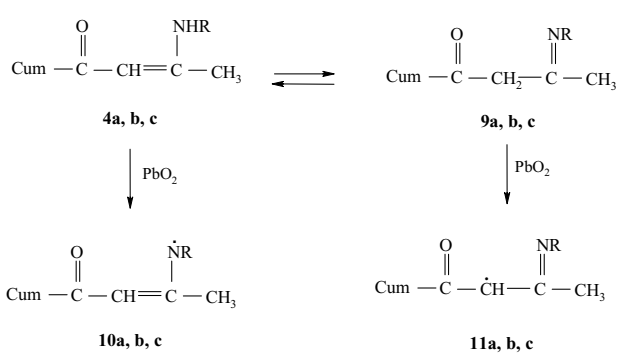

Scheme 2

10), also the abstraction from –CH_2- group (radical **11**) has to be considered (Scheme 2).

The experimental EPR spectrum of **12a** was simulated (Fig. 3.) using the splitting constants (1 . a_N(NO) = 1.03 mT,

1 . a_N = 0.28 mT, 3 . a_H(*o, p*) = 0.256 mT, 2 . a_H = 0.085 mT), which seemingly document that NH-group underwent an homolytic fission. Produced aminyl radical **10** adds immediately to spin trap under the formation of adduct **12**. Nevertheless, the EPR spectrum was also simulated using the EPR parameters (1 . a_N(NO) = 1.03 mT, 1 . a_H = 0.56 mT, 3 . a_H(*o, p*) = 0.256 mT, 2 . a_H(m) = 0.085 mT), i. e. the splitting 1 . a_N = 0.28 mT was replaced by two times greater splitting 1 . a_H = 0.56 mT (adduct **13**). Although in both simulations theoretically different intensities of lines should be expected, due to the uncomplete quality of experimental EPR spectrum it is difficult to distinguish between this two alternatives. Therefore, also the addition of C-radical has also be taken into account (Scheme 3).

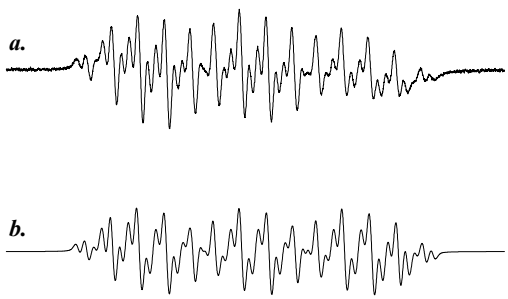

Fig. 3. **Experimental (a) and simulated (b) EPR spectrum of radical adduct** 12a **in nitrosobenzene**

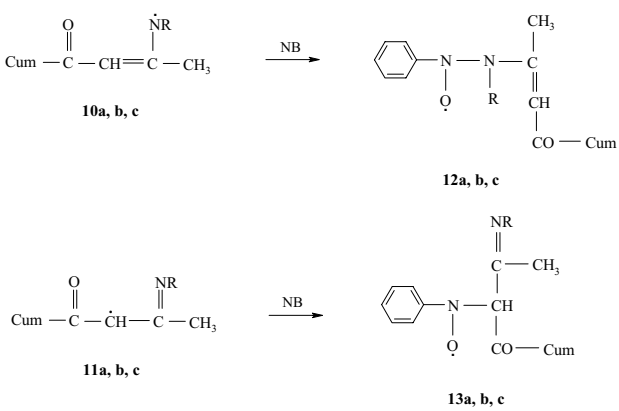

Scheme 3

Considering the above menthioned behaviour of enaminoketones **4**, it was also of interest to examine affinity of the N-H bond towards other radical reagents. Peroxyradicals were generated by decomposition of tertbutylhydroperoxid in heterogeneous system on the surface of PbO_2 or in homogeneous system by mixing with benzene solution of $Co(acac)_2$. In the absence of spin trap no EPR spectra of nitroxyl radicals, the products of the oxidation of NH group were registered. On the other hand, in the presence of spin trap only EPR spectra of radical adducts of $RO_2^{\cdot}$ radicals were observed. This can be attributed to the fact that either the enamine double C = C bond in **4a–4c** is preferentially attacked, or the tautomeric form **9** having no NH bond is predominantly present in the solution (see above).

The compound **5**, a benzolog of **1**, exhibits generally identical properties. The EPR spectrum of its radical with nitrosobenzene is shown in Fig. 4. Corresponding parameters (1 . a_N(NO) = 1.009 mT, 1 . a_H = 0.495 mT, 3 . a_H(*o, p*) = 0.262 mT, 2 . a_H(*m*) = 0.090 mT) do not significantly differ from those obtained from structure **1a–1b**. The EPR parameters of adducts with other spin traps such as nitrosotoluene and 2-methyl-2-nitrosopropane (2-methyl-2-nitrosopropane: 1 . a_N(NO) = 1.333 mT, 1 . a_H = 0.453 mT; nitrosotoluene: 1 . a_N(NO) = 1.115 mT, 2 . a_H(*o, p*) = 0.180 mT, 3 . a_H(CH_3) = 0.180 mT, 2 . a_H(*m*) = 0.080 mT, 1 . a_H = = 0.413 mT) are essentially identical. This indicates that the annelation of the coumarin skeleton by further phenyl ring did not change the character of behaviour of tricyclic derivative **5** on PbO_2 surface when compared with parent compound **1**.

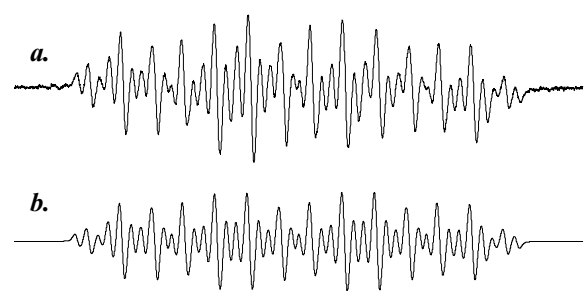

Fig. 4. **Experimental (a) and simulated (b) EPR spectrum of radical adduct from** 5 **with nitrosobezene**

EPR measurement of benzopyrano [4,3–b] pyridines **6** on the surface of PbO_2 does not lead to detection of any radical products even in the presence of spin trap. No radical formation was also observed upon the peroxylradical treatment.

Conclusion

Spin trapping technique was applied for the detection of radical intermediates generated from substituted coumarins during the decomposition on PbO_2 surface. Carbon centred radicals are generated from 3-acetoacetyl substituted coumarins. The nitrogen centred radicals are supposed to be formed by the decomposition of 3-amino derivatives, although also the second alternative, formation of carbon centred radicals, cannot be excluded.

REFERENCES

1. Světlík J.: J. Heterocyclic Chem. *37*, 395 (2000).
2 Booth B. L., Edge D. J., Haszeldine R. N., Holmes R. G. G.: J. Chem. Soc., Perkin Trans. *2*, 7 (1997).
3. Omelka L., Kluge R., Reinhardt M., Schulz M.,: J. Prakt. Chem. *330*, 510 (1998).
4. Thomas J.: J. Am. Chem. Soc. *82*, 5955 (1960).

L06 SPATIAL PROFILING OF DEGRADATION PROCESSES IN HINDERED-AMINE-STABILIZED POLYMERS BY ELECTRON SPIN RESONANCE IMAGING OF NITROXIDES

ANTONÍN MAREK, LUDMILA KAPRÁLKOVÁ, JIŘÍ PFLEGER, JAN POSPÍŠIL and JAN PILAŘ
Institute of Macromolecular Chemistry, Academy of Sciences of the Czech Republic, Heyrovského Sq. 2, 162 06 Prague 6, Czech Republic, pilar@imc.cas.cz

Introduction

Various organic polymeric materials such as plastics, fibers, elastomers, coatings, polymer blends and blends containing recyclates are vulnerable during outdoor application to environmental physical and chemical attacks. The relevant degradation processes resulting in deterioration of engineering properties of polymers and limiting their service lifetime are classified as long-term heat aging and weathering[1]. The latter is a rather complex process[2–4] triggered by solar radiation, temperature, mechanical forces or chemical catalysis[5,6]. The actinic part of solar radiation, including a part of UV-B (295–315 nm) and full range of UV-A (315–400 nm) radiation, is the most dangerous component of weathering. Air oxygen and oxidizing atmospheric pollutants (ozone and nitrogen oxides) are, together with atmospheric humidity and acid pollutants, the principal chemical climatic deteriogens attacking polymers during weathering[6].

The overall chemical free-radical chain mechanism of photooxidation of carbon-chain polymers, polyolefins and styrenics in particular, involves[7–9] formation of C-centered radicals in the initiation step and formation of polymeric alkylperoxy radicals $POO^{\bullet}$ and polymeric hydroperoxides POOH in the propagation step. The latter are a strong chromophoric impurity[7,8,10] increasing the sensitivity of saturated carbon-chain polymers to further photooxidation[11]. Hydroperoxides are photolyzed by the UV part of solar radiation into polymeric alkoxy radicals $PO^{\bullet}$. The latter are involved in chain branching, chain scission and formation of polymer-chain-bound carbonyl species > C = O[12–14]. Carbonyls are another chromophoric impurity accumulating in weathered carbon-chain polymers together with other oxygenated products[11,15].

Synthetic polymers have – contrary to living systems – no inherent natural power to remedy structural defects arising by photooxidation. Hence, application of properly selected stabilizing additives is necessary to enable a proper outdoor exploitation of polymers. Protecting polymers against photooxidative degradation[7,16,17] requires preventive stabilization by UV absorbers (UVAbs), deactivation of peroxidic species by amine-based photoantioxidants (hindered amine stabilizers, HAS) and quenching of photoexcited states. UVAbs and HAS are of general importance. The former protect polymers by preferential absorption of harmful solar radiation and limit in this way initiation of photodegradation by preventing photolysis of POOH and photosensitization by excited carbonyl groups.[16,18]

Activity of HAS has a curative character. The generally accepted stabilizing mechanism for secondary HAS (having the > NH group in the molecule) is interpreted as deactivation of hydroperoxides POOH (Eq. 1) followed by formation of either hydroxylamine (Eq. 2a) or *O*-alkylhydroxylamine (Eq. 2b). Both the species are oxidized in a sacrificial stabilization process by alkylperoxy radicals to HAS-derived nitroxides,[16–18] (Eqs. 3, 4), the key transformation product in the integral cyclic stabilization mechanism of HAS. Nitroxides scavenge C-centered radicals $P^{\bullet}$ (Eq. 5) in a process competing with their oxidation or self-reactions[19,20]. The formed *O*-alkylhydroxylamine is able to deactivate another alkylperoxyl, without depletion of the HAS activity or formation of any peroxidic product from the polymer[16,21,22] (Eq 4). The cyclic process >NH → $>NO^{\bullet}$ → >NOP → $>NO^{\bullet}$→ >NOP etc. has been considered as responsible for the high efficiency and durability of HAS in photooxidizing polymers. Nitroxides are formed from tertiary HAS (having $>NCH_3$ as active group) or *N*-acyl-HAS (with $>NCOCH_3$ group) as well[23,24]. Direct scavenging of alkylperoxyls is assumed in application of HAS having structures of *O*-alkylhydroxylamines.

$$>NH + POOH \longrightarrow [>NH \cdots HOOP] \quad (1)$$

$$[>NH \cdots HOOP] \xrightarrow{h\nu} >NOH + POH \quad (2a)$$

$$[>NH \cdots HOOP] \xrightarrow{h\nu} >NOP + HOH \quad (2b)$$

$$>NOH + POO^{\bullet} \longrightarrow >NO^{\bullet} + POOH \quad (3)$$

$$>NOP + POO^{\bullet} \longrightarrow >NO^{\bullet} + POH + P^{1}COP^{2} \quad (4)$$

$$>NO^{\bullet} + P^{\bullet} \longrightarrow >NOP \quad (5)$$

Molecular and morphological changes arising by photooxidation have heterogeneous character.[5,25–28] Concentration gradients from the surface into the polymer bulk arise due to diffusion-limited oxidation[29] and the effect of radiation. Shyichuk et al[30–33]. studied the chain-scission and crosslinking rates in polypropylene (PP) and polystyrene (PS) plaques after UV exposure using GPC to assess the effect of degradation on molecular weight distribution. They found that concentrations of both scissions and crosslinks are high at the illuminated surface, decrease in the interior, and increase again at the unexposed surface. The data clearly indicate that there was practically no difference in concentrations between irradiated and unexposed surfaces of PP. But, in the case of PS, much lower concentrations (less than 50 %) were found at the unexposed surface compared with the irradiated surface. It was found that the intensity of UV radiation in PP and PS plaques diminishes as the UV light penetrates deeper into the material. The transmitted UV radiation level at the unexposed surface of PP was found to be only about 4 % of that at the exposed surface compared with 33 % in the case

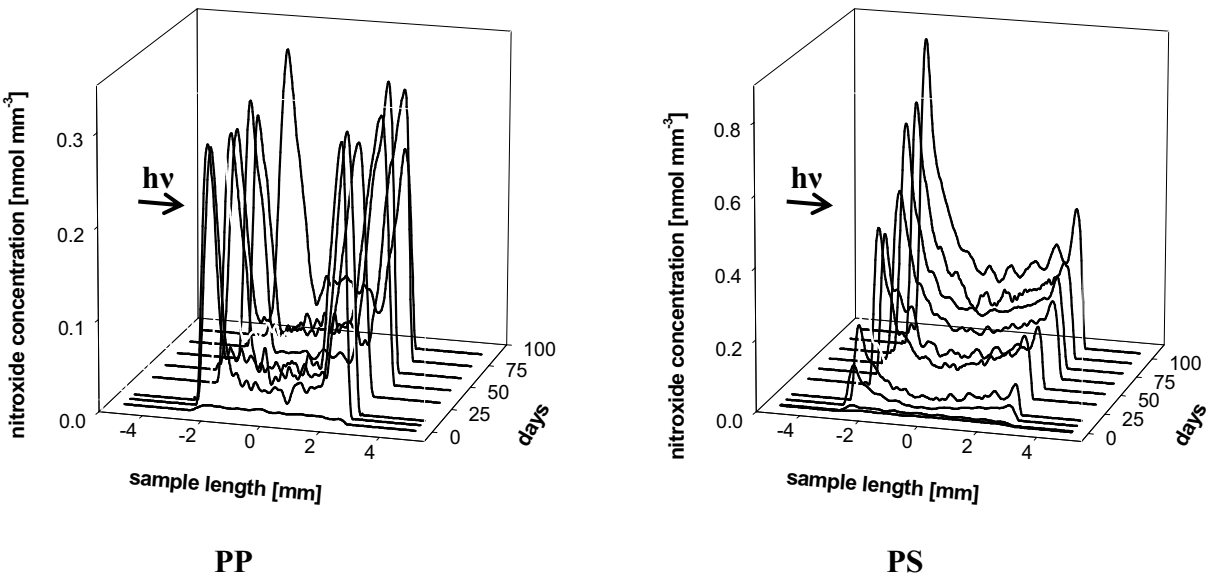

Fig. 1. **Dependence of nitroxide concentration profiles in PP and PS plaques stabilized with 1 wt % of Tinuvin®770 and exposed to accelerated photodegradation on the exposure time**

of PS[30]. It follows that an uneven distribution of formed nitroxides is expected and that its experimental determination can bring important information on the heterogeneity of the degradation process.

Electron spin resonance (ESR) spectroscopy is a highly selective and non-destructive powerful technique which is able to supply data on concentration, structure, and some other properties of paramagnetic compounds including free radicals and HAS-derived nitroxides. Electron spin resonance imaging (ESRI) that is one of the most advanced ESR techniques is able to provide information on spatial distribution of paramagnetic compounds in studied samples[34]. The results of pioneering ESRI studies of spatial resolution of photodegradation processes have been published by Lucarini et al[35–37]. Who determined the time-dependence of concentration profiles of nitroxides during weathering of PP in the presence of various HAS. They used a simple back-projection technique and found various shapes of concentration profiles of nitroxides in PP samples in dependence on time and the additives used (HAS and UV absorbers). Recent papers by Franchi et al[38]. And by Lucarini et al[39]. Report results of a series of ESRI experiments on PP during long-term (up to six months) degradation in the presence of two different HAS.

Experimental

Polystyrene (PS) and polypropylene (PP) 6 mm thick plaques containing 1.0 wt% of HAS stabilizers and their mixtures with other photostabilizers were prepared and subjected to accelerated weathering in an Atlas Ci3000 + weatherometer (295–800 nm, black panel temperature 60 °C) and to an oven test (60 °C). Cylindrical samples (diameter 3 mm, length 6 mm) were made of the plaques after appropriate time periods of exposition. The time dependence of the concentration profiles of nitroxides generated in the plaques along the axes of the cylinders coinciding with the direction of irradiation incident upon the surface in the weatherometer was determined by the ESRI technique using a Bruker ELEXSYS E540 spectrometer with gradient coils. The carbonyl and hydroxy groups on both surfaces and inside the plaques were identified by ATR FTIR. The spectra were measured on a Bruker IFS-55 spectrometer with MCT detector, using an ATR Golden Gate Specac device with MKII Diamond ATR Top Plate. Optical transparency spectra of polymer plaques were measured with PerkinElmer Lambda 950 spectrophotometer equipped with a 60 mm integrating sphere, which makes it possible to include contribution of the light scattered by crystalline domains present in PP.

Results and Discussion

Different shapes of nitroxide concentration profiles along the direction of light incident perpendicularly upon the surface of the plaques were found[40] in PP and PS stabilized with Tinuvin®770 and exposed to long-term accelerated weathering (simultaneous photo- and thermodegradation) or oven test (thermodegradation) when protected with various HAS-based stabilization systems (Fig. 1.). The U-shaped profiles, showing approximately the same concentrations of nitroxides in both irradiated and unexposed surface layers of the plaques and significantly lower concentrations of nitroxides generated in the bulk were found in PP. In contrast, the irradiated surface layers of PS plaques contained higher nitroxide concentrations than the unexposed ones. Similar concentration gradients of principal polymer oxygenated products, carbonyl and hydroxy groups were found by ATR FTIR.

By measurement of optical transparency spectra of polymer plaques using an integrating sphere technique we found that the photodegraded PP is more transparent for the actinic part of the solar radiation (wavelengths 295–400 nm) than the photodegraded PS (Fig. 2.). This finding indicates that the intensity of light penetrating into the plaque and, consequently, the concentration of photoactivated centers of degradation decreases with increasing distance from the irradiated surface of the sample, more steeply in PS than in PP.

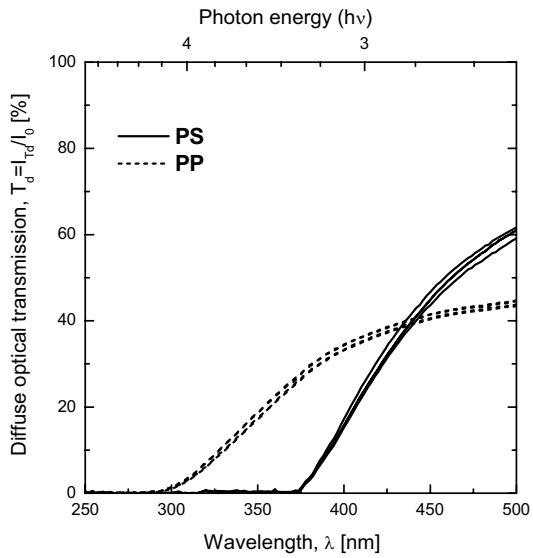

Fig. 2. **Diffusion transmission spectra of the PP and PS plaques stabilized with 1.0 wt % of Tinuvin®770 and exposed to accelerated photodegradation for 87 and 106 days, respectively**

Significant differences in the shapes of nitroxide concentration profiles were found and explained also in PP and PS protected with other HAS-based stabilization systems containing UV absorbers and phenolic antioxidants. The results were explained considering the mechanisms of activity of various components of the systems.

Our results (shape and time dependence of concentration profiles of nitroxides) are not in agreement with the mentioned results of studies performed by Lucarini group[35–39] under similar experimental conditions. Some disagreement may be due to the large dimensions (in particular length) of their samples which may exceed the volume in which the gradient field is uniform.

Very low concentrations and practically homogeneous distribution of nitroxides were found in PS samples stabilized with Tinuvin®770 as a sole additive, which were exposed to oven test. The result confirms high thermal stability of PS. A slightly higher concentration of homogeneously distributed nitroxides, but still significantly lower than observed in the samples exposed to accelerated photodegradation, was found in PP samples stabilized with Tinuvin®770 as a sole additive, which were exposed to oven test.

Conclusions

The observed shapes of nitroxide concentration profiles can be interpreted as a result of a superposition of the effect of the diffusion-limited oxidation, which is responsible for the low nitroxide concentration in the polymer bulk, and the effect of the different concentration gradients of photoactivated degradation centers in PP and in PS.

This research was supported by the Academy of Sciences of the Czech Republic (project AVOZ 40500505).

REFERENCES

1. White J. R.: Plast. Rubber Compos. Process. Appl. *27*, 124 (1998).
2. Searle N. D. in: *Encyclopedia of Polymer Science and Engineering, 17*, 786 (1989).
3. Wypych G.: *Handbook of Material Weathering,* 2nd ed., ChemTec Publishing, Toronto 1995.
4. Kockott D. in: *Handbook of Polymer Testing. Physical Methods.* (Brown R., Ed.), p. 697. Rapra Technology, Shawbury 1989.
5. White J. R., Trurnbull A.: J. Mater. Sci. *29*, 584 (1994).
6. Pospíšil J., Pilař J., Billingham N. C., Marek A., Kruliš Z., Nešpůrek S., Habicher W. D.: In: *Natural and Artificial Ageing of Polymers* (Reichert T., Ed.), p. 411. Gesellschaft für Umweltsimulation e. V. GUS, Pfinztal, Germany, 2004.
7. Rabek J. F.: *Polymer Photodegradation: Mechanisms and Experimental Methods.* Chapman & Hall, London 1995.
8. Pospíšil J.: Chem. Listy *85*, 904 (1991).
9. Ranby B., Rabek J. F.: *Photodegradation, Photo-oxidation and Stabilization of Polymers.* J. Wiley & Sons, London 1975.
10. Wiles D. M., Carlsson D. J.: Polym. Degrad. Stab. *3*, 61 (1980–1).
11. Carlsson D J. Wiles D. M.: Macromolecules *2*, 587 (1969).
12. Ginhac J. M., Gardette J. L., Arnaud R., Lemaire J.: Macromol. Chem. *182*, 1017 (1981).
13. Pospíšil J., Rosík L., Nešpůrek S.: Plasty Kauc. *34*, 324 (1997).
14. Wendelt B.: Eur. Polym. J. *22*, 755 (1986).
15. Pospíšil J., Horák Z., Kruliš Z., Nešpůrek S.: Macromol. Symp. *135*, 247 (1998).
16. Pospíšil J., Nešpůrek S.: Prog. Polym. Sci. *25*, 1261 (2000).
17. Pospíšil J.: Adv. Polym. Sci. *124*, 87 (1995).
18. Pospíšil J., Nešpůrek S., in: *Handbook of Polymer Degradation* (Hamid S. H., Ed.), 2nd ed., p. 191. Dekker, New York 2000.
19. Chateaunef J., Lusztyk J., Ingold K. U.: J. Org. Chem. *53*, 1629 (1988).
20. Beckwith L. J., Bowry V. W., Ingold K. U.: J. Am. Chem. Soc. *114*, 4983 (1992).

21. Klemchuk P. P., Gande M. E.: Makromol. Chem., Macromol. Symp. *28*, 117 (1989).
22. Step N. E., Turro N. J., Gande M. E., Klemchuk P. P.: Macromolecules *27*, 2529 (1994).
23. Gugumus F.: Polym. Degrad. Stab. *34*, 205 (1991).
24. Kurumada T., Ohsawa H., Fujita T., Toda T., Yoshioka T.: J. Polym. Sci., Polym. Chem. Ed. *72*, 277 (1984).
25. Billingham N. C.: Macromol Chem., Macromol. Symp. *29*, 145 (1989).
26. Rabello M. S., White J. R.: Polym. Degrad. Stab. *56*, 55 (1997).
27. George G. A., Celina M., in: *Handbook of Polymer Degradation* (Hamid S. H., Ed.), 2nd ed., p. 277. M. Dekker, New York 2000.
28. Billingham N. C.,: In: *Plastics Additives Handbook* (Zweifel H., Ed.), 5th ed., p. 1017. Hanser Publishers, Munich 2001.
29. Audouin L., Langlois V., Verdu J., de Bruin J. C. M.: J. Mater. Sci. *29*, 569 (1994).
30. Shyichuk A. V., Melnyk D., White J. R.: J. Polym. Sci., Part A, Polym. Chem. *41*, 1070 (2003).
31. Shyichuk A. V., Stavychna D. Y., White J. R.: Polym. Degrad. Stab. *72*, 279 (2001).
32. Shyichuk A. V., White J. R.: J. Appl. Polym. Sci. *77*, 3015 (2000).
33. Shyichuk A. V., White J. R., Craig J. H., Syrotynska I. D.: Polym. Degrad. Stab. *88*, 415 (2005).
34. *EPR Imaging and in vivo EPR* (Eaton G. R., Eaton S. S., Ohno K., Eds.). CRC Press, Boca Raton, 1991.
35. Lucarini M., Pedulli G. F., Borzatta V., Lelli N.: Polym. Degrad. Stab. *53*, 9 (1996).
36. Lucarini M., Pedulli G. F., Borzatta V., Lelli N.: Res. Chem. Intermed. *22*, 581 (1996).
37. Lucarini M., Pedulli G. F.: Angew. Makromol. Chem., *252*, 179 (1997).
38. Franchi P., Lucarini M., Pedulli G. F., Bonora M., Vitali M.: Macromol. Chem. Phys. *202*, 1246 (2001).
39. Lucarini M., Pedulli G. F., Motyakin M. V., Schlick S.: Prog. Polym. Sci. *28*, 331 (2003).
40. Marek A., Kaprálková L., Schmidt P., Pfleger J., Humlíček J., Pospíšil J., Pilař J.: Polym. Degrad. Stab., in press.

L07 ESR STUDY OF DIFFUSION PROCESSES IN POLY(2-HYDROXYETHYL METHACRYLATE) GELS AND CONCENTRATED SOLUTIONS

ANTONÍN MAREK, JAN PILAŘ and JIŘÍ LABSKÝ
Institute of Macromolecular Chemistry, Academy of Sciences of the Czech Republic, Heyrovský Sq. 2, 162 06 Prague 6, Czech Republic, marek@imc.cas.cz

Introduction

As an alternative to the rotational diffusion of nitroxide spin-labels[1,2], ESR can also provide the information on macroscopic translational diffusion of spin probes[3–10]. For this purpose the spectrometer has to be equipped with gradient coils producing an additional gradient field and along its direction a spatial resolution can be achieved. Spin probes are then used as tracers diffusing in the system studied and ESR spectrometer serves as a sensitive microscopic tool for detection of the spatial distribution of tracer. For the purpose of estimation of tracer diffusion coefficients it is sufficient to simulate a one-dimensional diffusion, i. e. one-dimensional electron spin resonance imaging (1D ESRI). In this case the 1D tracer concentration profile can be estimated by simple deconvolution[4] of the ESR spectrum taken with the gradient coils-off out of the spectrum taken with gradient coils-on. Macroscopic measurements are, in general, interpreted in terms of a simple phenomenological description of diffusion given by Fick's second law[11].

The purpose of the present study is to show the ability of ESR analysis to provide reliable results in the interesting region of semidilute and more concentrated solutions as well as in swollen polymer networks (polymer gels). Comparison of tracer mobility in gels with that in non-crosslinked polymer solutions[8–10,12,13] can provide an important insight into the diffusion mechanism in both situations, with direct impact on practical applications such as drug delivery systems and transport across membranes. Despite several diffusion models[14,15] trying to explain diffusion of low-molecular weight tracers in concentrated solution, a consensus has not been attained yet[16]. Especially in the case of gels, reliable data are comparatively sparse and diffusion mechanism are unsatisfactorily explained.

Experimental

Poly (HEMA) solutions, gels and paramagnetic tracers. Methanolic solutions of poly (2-hydroxyethyl methacrylate) (poly (HEMA)) were prepared by dissolving appropriate amounts of commercial polymer (Polysciences Inc.) in a closed vessel until homogenous highly viscous solutions were obtained. Gel chromatography performed in dimethylacetamide using polystyrene standards showed $M_w \sim 1\,000\,000$ and a very high polydispersity (> 4) of this polymer.

HEMA gels (**III**) (Chart 1) were prepared by polymerizing a mixture of 2-hydroxyethyl methacrylate (**I**) (containing a persistent amount of 0.12 % of ethylene dimethacrylate crosslinker as determined by gas chromatography), ethylene dimethacrylate crosslinker (**II**), 2,2´-azobis(2-methylpropanenitrile) initiator (Fluka), and methanol in proper proportions (Table I). For ESRI experiments the mixture was filled into glass capillary tubes (i. d. about 1 mm) and larger glass ampoules (i. d. about 10 mm) for light scattering and swelling experiments. Capillaries and ampoules were sealed and the reaction mixture was polymerized at 65 °C for 8 h. Swelling was monitored by weighing the sample until equilibrium was reached. Three types of gels were prepared by polymerization in the presence of an amount of methanol required for equilibrium swelling (Table I).

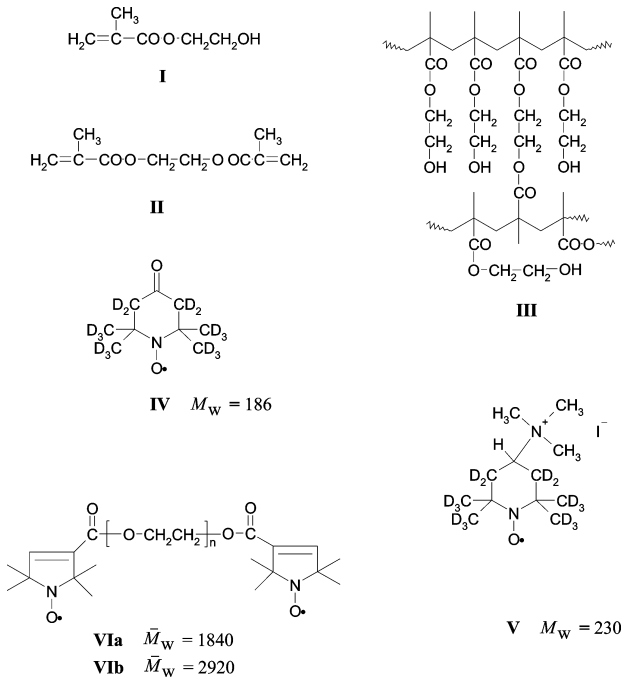

Chart 1

Table I
Characterization of Poly (2-hydroxyethyl methacrylate) Gels (G) and Solutions (S) in Methanol Used in Diffusion Studies

Code	c_H[wt%][a]/c_c[wt%][b]	c[g ml^{-1}][c]	$\Phi . 10^3$[d]	L_H[nm]
G23	23/0.7	0.201	158	6.7[e]
G29	29/3.5	0.255	200	4.1[e]
G35	35/3.8	0.323	254	3.2[e]
S02	0.2	0.00158	1.24	10.3[f]
S05	0.5	0.00396	3.11	10.5[f]
S1	1	0.00794	6.23	10.3[f]
S2	2	0.0159	12.5	10.4[f]
S5	5	0.0403	31.6	10.6[f]
S10	13	0.0822	64.5	9.8[f]
S23	23	0.199	156	6.9[e]
S29	29	0.258	202	6.0[e]
S35	35	0.319	251	5.1[e]
S50	50	0.488	383	2.9[e]

[a]Polymer weight fraction (without crosslinker in case of gels). [b]Crosslinker weight fraction. [c,d]Polymer concentration and volume fraction, respectively (within crosslinker in case of gels). [e]Hydrodynamic correlation length determined by DLS in gels and nondilute solutions. [f]Hydrodynamic radius R_H determined by DLS in dilute solutions

The synthesis of paramagnetic tracers used in the study (**IV–VI**) was described[9,10] previously. The tracers **VI a, b** were characterized by MALDI-TOF mass spectrometry (Biflex III, Bruker Daltonik, Bremen, Germany). Molecula weight ratios $\bar{M}_w/\bar{M}_n$ for tracers **VI a** and **VI b** were 1840/1800 and 2920/2900, respectively.

Dynamic Light Scattering (DLS). Poly(HEMA) gels and solutions in glass ampoules (i. d. about 10 mm) were used for DLS experiments. The correlation functions were analyzed using the REPES program[17,18]. The collective diffusion coefficients, D_c, of concentrated solutions and gels were calculated in a standard way from the mean characteristic decay times using the expression $D_c = 1/\tau_c q^2(1–\Phi)^2$, where τ_c is the mean characteristic decay time, $q = 4\pi n_0 \sin(\theta/2)/\lambda_0$ is the magnitude of the scattering vector, n_0 is the refractive index of the solvent, and λ_0 is the wavelength of the incident light. In this expression, a correction for solvent back-flow[19] is made, (division by $(1–\Phi)^2$, where Φ is the polymer volume fraction, $\Phi = \bar{v}_2 c$, $\bar{v}_2 = 0.785$ cm^3 g^{-1} is the partial specific volume[20] of poly (HEMA) and c, g ml^{-1}, is the polymer concentration). D_c for gels was further corrected by the heterodyne method introduced by Geissler[21]. Then the concentrated polymer solutions and gels were characterized by the dynamic correlation length, L_H, using the Stokes-Einstein relation, $L_H = kT/6\pi\eta D_c$, where T is the absolute temperature, k is the Boltzmann constant and η the viscosity of the solvent. The L_H is identified with hydrodynamic radius R_H in dilute solutions and with dynamic correlation length (hydrodynamic blob size) ξ_H in semidilute solutions and in gels.

ESRI. For ESRI measurements we used poly (HEMA) gel and solution samples in glass capillaries tubes (i. d. ca 1 mm). The sample lengths ranged from 3 to 10 mm. The diffusion was started with ca 0.2 μl of 0.05 M methanolic solution of a paramagnetic tracer. The capillary was then inserted into an ESR quartz sample tube (4 mm o. d.) and placed, with its axis parallel to the vertical gradient direction, in the cavity of ESR spectrometer.

With gels, the tracer solution was simply topped on the gel. A different experimental arrangement was used for measurements in polymer solutions. The diffusion was started as in the case of gel but then the tracer was over layered with a polymer solution ("sandwich" arrangement). Generally, the "sandwich" arrangement provides data that could be more precisely analyzed.

The ESRI system in the Detroit laboratory consists of a Bruker 200D ESR spectrometer with an EMX console, equipped with two eight-shaped Lewis coils fed by two regulated power supplies. Measurements were performed using a vertical gradient (perpendicular to the external magnetic field); 50–150 G cm^{-1}. The instrumentation has been described in more detail elsewhere[8–10]. All the measurements were performed at a stabilized temperature of 300±1 K.

Data Analysis

Determination of Experimental Concentration Profiles by Deconvolution Techniques. For deconvolution, a well-known numerical problem, many methods have been developed so far[22]. In practice, noise is always present in any physical measurement and the naive direct linear approach

produces poor results. The only way of a robust solution, independent of noise, is the use of nonlinear methods, which utilize some kind of prior knowledge of the concentration profile in the form of physically meaningful constraints, such as the condition of positivity, finite extent, or maximum likelihood or entropy. In this work we used a combination of three deconvolution methods. First approach is based on the fast Fourier deconvolution method, which is followed by noise filtering[23] and frequency restoration beyond the cutoff[24–26]. The resulting profile can be further subjected to a deconvolution method based on a Monte Carlo optimization routine, which uses the well known Metropolis algorithm[22]. A rigorous approach to seeking the unique solution with desired features is Frieden's method of maximum likelihood[22,27]. Unfortunately, even its simple form, the maximum entropy method, requires much computer time.

Estimation of Diffusion Coefficient by Fitting 1D Tracer Concentration Profile. On the assumption that the concentration of the tracer inside the sample is sufficiently low so that the translational diffusion obeys Fick's Law $\partial C(\vec{\mathbf{r}},t)/\partial t = D\Delta C(\vec{\mathbf{r}},t)$ and if the diffusion along the capillary axis strongly predominates over those in other directions, we may write the solution of this equation as a 1D spatial and time dependence of the tracer concentration

$$C(x,t) = \frac{1}{(4\pi Dt)^{1/2}} \int_{-\infty}^{+\infty} e^{-(x-x')^2/4Dt} C(x',t=0)\mathrm{d}x'$$

where D is a diffusion coefficient and x is a space coordinate along the gradient direction, for an arbitrary initial tracer distribution[11].

Once we have found a time series of concentration profiles of the tracer in the sample, it is advantageous to take a previous profile as starting for a later profile. If the diffusion follows Fick's Law, combinations of different pairs of concentration profiles should give the same diffusion coefficient. The plot of Dt vs. t could be fitted with a straight line crossing the origin, and its slope gives coefficient D.

Results and discussion

Sample Characterization. The hydrodynamic correlation lengths, L_H, determined for gels and solutions studied by DLS are given in Table I. The crossover concentration at which the overlap of the polymer coils begins, was estimated $c^* = 0.11$ g ml^{-1}. It follows from Table I that ξ_H found in concentrated poly (HEMA) solutions is systematically larger than ξ_H in gels containing the same polymer volume fraction Φ. This result can be explained on the basis of the theory of Tanaka[28], according to which the smaller blob size is caused by an additional elastic modulus in gels due to the presence of permanent crrosslinks.

Dependence of Diffusion Coefficients on Matrix Properties. In nondilute solutions, changes in local friction with changing polymer concentration can exert a significant influence on D. To account for the local friction, the D values presented in Table II were scaled by the ratio $\xi(c)/\xi(0) = (1+\phi)2/(1-\phi)$, where φ is the polymer volume fraction, in the way used and discussed by Wheeler and Lodge[16].

The dependence of corrected diffusion coefficients of the tracers on the poly (HEMA) concentration in methanolic solution, which was in all the matrices presented in Table II well above c^*, was analyzed in the frame of Phillies'[15] and Petit's[14] models. The respective equation for the tracer diffusion coefficient is given by relations $D = D_0 \exp(-\alpha_1 c^{\nu_1})$ and $D = D_0/(1+\alpha_2 c^{2\nu_2})$, where D_0 is the diffusion coefficient of the tracer in the absence of the polymer, c is the polymer concentration and α, ν are the model parameters. The best-fit parameters are presented in Table III. Both models

Table II
Diffusion Coefficients $D.10^8$ [cm^2 s^{-1}] of Paramagnetic Tracers IV–VI in Poly (2-hydroxyethyl methacrylate) Gels and Solutions in Methanol

Code	c[a] [g ml^{-1}]	IV		V		VIa		VIb	
		D	D_{corr}[b]	D	D_{corr}[b]	D	D_{corr}[b]	D	D_{corr}[b]
G23	0.201	240	380	100	160	29	46	31	50
G29	0.255	–	–	–	–	16	29	8.8	16
G35	0.323	120	250	63	130	6.6	14	5.5	11
S15	0.126	797	1070	612	820	164	220	107	144
S20	0.171	642	954	448	666	144	214	–	–
S23	0.199	591	936	–	–	95.7	152	67.9	108
S30	0.268	451	837	266	494	57.9	107	39.0	72.4
S35	0.319	347	724	210	438	36.5	76.1	25.2	52.6
S36	0.330	325	695	177	379	35.8	76.6	19.8	42.4
S40	0.373	244	576	127	300	25.6	60.5	12.7	30.0
S45	0.429	168	453	89.8	242	15.9	42.8	8.23	22.2

[a]Polymer concentration (within crosslinker in case of gels). [b]Values corrected for local solvent friction in the matrix (see the text)

fit the experimental data well at a similar level of accuracy (Fig. 1.).

Diffusion coefficients of the tracers measured in HEMA gels corrected in the same way as those measured in solutions are presented in Fig. 1. for comparison. Lower diffusion coefficients measured in HEMA gels compared with poly (HEMA) solutions in matrices with the same polymer concentration follow from Fig. 1. One of the reasons is the smaller ξ_H found in HEMA gels when compared with poly (HEMA) solutions at the same polymer concentration (Table I). However, this effect cannot quantitatively explain the observed decrease in the tracer diffusion coefficients. In

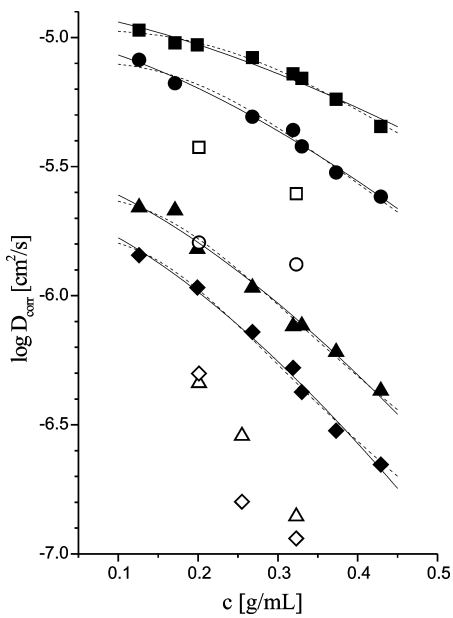

Fig. 1 **Dependence of the corrected diffusion coefficients of the tracers on the polymer concentration in methanolic solutions of poly(HEMA) (■ IV, ● V, ▲ VIa, ◆ VIb) and in HEMA gels equilibrium-swollen with methanol (open symbols). Best fits to the data for particular tracers in concentrated solutions calculated using Phillies' and Petit's models and the parameters given in Table III are shown by solid and dashed lines, respectively**

lightly crosslinked gel G23 (c = 0.201 g ml^{-1}), only minor differences in hydrodynamic correlation lengths were measured compared with solution S23. Nevertheless, practically the same relative decrease in diffusion coefficients for all four tracers was observed when comparing both mentioned matrices. It is impossible to explain this difference on the basis of the monodisperse scaling theory and other models based on the single correlation length, whether hydrodynamic in Phillies' model or obstruction interactions in Petit's model are taken into account.

Fig. 2. presents the collective diffusion peaks of sample S23 and G23. Whereas the mean values of ξ_H are identical for both samples, the distribution of correlation lengths is much broader in the gel than in the solution. This broad distribution in gels is one of the signs of large scale imperfections in gels followed by submicrometer concentration heterogeneities forming additional obstacles or traps[29], which are known to influence transport properties through gels. Heterogeneities are also responsible for the need of heterodyne corrections in DLS measurements as well as the observations of the typical "speckle" pattern.

Table III
Best-fit Parameters of Phillies' and Petit's Models for Concentration Dependence of Diffusion Coefficients of Paramagnetic Tracers in Poly (2-hydroxyethyl methacrylate) Methanolic Solutions

Tracer	Phillies' model: $D = D_0 \exp(-\alpha_1 c^{\nu_1})$			Petit's model: $D = D_0/(1+\alpha_2 c^{2\nu_2})$		
	D_0 [10^{-6}cm^2/s]	α_1	ν_1	D_0 [10^{-6}cm^2/s]	α_2	ν_2
IV	13	3.4	1.48	11	18	1.54
V	10	5.0	1.48	8.1	33	1.54
VIa	3.1	7.2	1.48	2.5	68	1.54
VIb	2.2	8.2	1.48	1.7	89	1.54

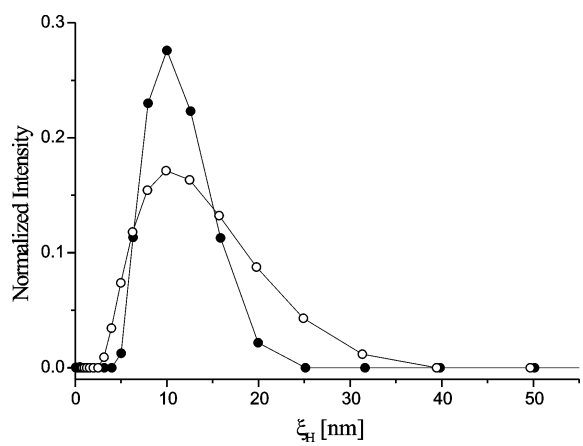

Fig. 2 **Distribution of correlation lengths in HEMA gel sample G23 (open symbols) and poly(HEMA) solution S23 (solid symbols) measured by DLS and evaluated by the program REPES using the Pearson fit to the correlation curve**

Conclusions

Suitable experimental arrangements for ESRI experiments aimed at determination of macroscopic translational diffusion of paramagnetic tracers in polymer solutions and gels were selected. Methods of treatment of experimental data based on deconvolution and fitting procedures were elaborated. Diffusion coefficients for four paramagnetic tracers in nondilute poly (HEMA) solutions in methanol and in HEMA gels equilibrium-swollen with methanol were determined.

Both solution and gel matrices were characterized by the hydrodynamic correlation length measured by DLS technique. The dependences of the corrected diffusion coefficients on the poly (HEMA) concentration in methanolic solutions were well fitted within the frame of both Phillies' and Petit's models at approximately the same level of accuracy. Lower values of diffusion coefficients for all four tracers were found in HEMA gels compared with polymer solutions containing the same concentration of the polymer. The data found indicate that slowing down of the tracer diffusion in gels depends not only on the presence of additional permanent crosslinks as demonstrated by shortening hydrodynamic screening length of the matrix but also on microscopic heterogeneities always present in gels. Experiments on similar systems are in progress to provide more reliable data especially for gel matrices.

This research was supported by the Grant Agency of the Academy of Sciences of the Czech Republic (project A4050306) and by the Polymers Program of the National Science Foundation, U.S.A. A. M. wishes to thank Prof. S. Schlick at University of Detroit Mercy, Detroit, MI, USA for hospitality and support in performing ESRI measurements.

REFERENCES

1. Pilar J., Labsky J., Marek A., Budil D. E., Earle K. A., Freed J. H.: Macromolecules *33*, 4438 (2000).
2. Marek A., Czernek J., Steinhart M., Labsky J., Stepanek P., Pilar J.: J. Phys. Chem. B *108*, 9482 (2004).
3. *EPR Imaging and in Vivo EPR* (Eaton G. R., Eaton S. S., Ohno K., eds.), CRC Press, Boca Raton, FL 1991.
4. Hornak J. P., Moscicki J. K., Schneider D. J., Freed J. H.: J. Chem. Phys. *84*, 3387 (1986).
5. Moscicki J. K., Shin Y. K., Freed J. H.: J. Chem. Phys. *99*, 634 (1993).
6. Moscicki J. K., Shin Y. K., Freed J. H.: J. Magn. Reson. *84*, 554 (1989).
7. Xu D. J., Hall E., Ober C. K., Moscicki J. K., Freed J. H.: J. Phys. Chem. *100*, 15856 (1996).
8. Gao Z., Pilar J., Schlick S.: J. Phys. Chem. *100*, 8430 (1996).
9. Pilar J., Labsky J., Marek A., Konak C., Schlick S.: Macromolecules *32*, 8230 (1999).
10. Schlick S., Pilar J., Kweon S. C., Vacik J., Gao Z., Labsky J.: Macromolecules *28*, 5780 (1995).
11. Crank J.: *The Mathematics of Diffusion,* Clarendon Press, Oxford, U.K. 1993.
12. Masaro L., Ousalem M., Baille W. E., Lessard D., Zhu X. X.: Macromolecules *32*, 4375 (1999).
13. Matsukawa S., Ando I.: Macromolecules *32*, 1865 (1999).
14. Petit J. M., Roux B., Zhu X. X., Macdonald P. M.: Macromolecules *29*, 6031 (1996).
15. Phillies G. D. J.: J. Phys. Chem. *93*, 5029 (1989).
16. Wheeler L. M., Lodge T. P.: Macromolecules *22*, 3399 (1989).
17. Štěpánek P., in: *Dynamic Light Scattering: The Method and Some Applications* (W. Brown, ed.), Oxford University Press, New York 1993.
18. Jakeš J.: Collect. Czech. Chem. Commun. *60*, 1781 (1995).
19. Vink H.: J. Chem. Soc., Faraday Trans. 1 *81*, 1725 (1985).
20. Vošický V., Bohdanecký M., Dušek K.: Collect. Czech. Chem. Commun. *44*, 1627 (1977).
21. Geisler E., in: *Dynamic Light Scattering: The Method and Some Applications* (W. Brown, ed.), Oxford University Press, New York 1993.
22. Jansson P. A.: *Deconvolution with Applications in Spectroscopy* Academic Press, Inc., London 1984.
23. *Matlab Signal Processing Toolbox.* The MathWorks, Natick, MA 1996
24. Howard S. J.: J. Opt. Soc. Am. *71*, 819 (1981).
25. Howard S. J.: J. Opt. Soc. Am. *71*, 95 (1981).
26. Howard S. J., in: *Deconvolution With Applications in Spectroscopy: Fourier Spectrum Continuation and Minimum-Negativity-Constrained Fourier Spectrum Continuation* (P. A. Jansson, ed.), Academic Press, Inc., London 1984.
27. Frieden B. R.: *Restoring with Maximum Likelihood.* Technical Report No. 67, Optical Sciences Center, University of Arizona, Tucson 1971.
28. Tanaka T., Hocker L. O., Benedek G. B.: J. Chem. Phys. *59*, 5151 (1973).
29. Bastide J., Leibler L.: Macromolecules *21*, 2647 (1988).

L08 ESR SPECTRA OF TITANOCENE AND ZIRCONOCENE COMPLEXES

MICHAL HORÁČEK
J. Heyrovský Institute of Physical Chemistry, Academy of Sciences of the Czech Republic, Dolejškova 3, 182 23 Prague 8, Czech Republic; horacek@jh-inst.cas.cz

Usefulness of ESR spectroscopy in titanocene and zirconocene chemistry will be demonstrated on three examples.

a) The efect of substitution on cyclopentadienyl ligand to acidity of titanium atom in titanocene monochloride complexes.

It has been well established that methyl substituents at the cyclopentadienyl ligands exert electron donation effects which result in a decrease of Lewis acidity at the metal centre. We have investigated such effects by ESR spectroscopy in a series of methylated titanocene monochloride compounds $[\eta^5\text{-}C_5H_{5-n}Me_n]_2TiCl$ (n = 0–5) containing titanium tri-valent[1]. These complexes have been prepared by the reduction of corresponding titanocene dichlorides by magnesium (Eq. 1). The donation effect of methyl group leads to the formation of monomeric titanocene complexes for trimethyl and more methylated ligand, whereas 0–2 methyl-substituted titanocene monochloride complexes are stabilized by coordination of solvent molecule or by formation of dimeric structures in non-coordinating solvents, respectively. The effect of methyl group on electron density of Ti is summarized in Table I.

The investigation of the influence of substitution on Cp ligands has been extended to the other groups having an electronic or steric effect. For example, the effect of the trimethylsilyl group in metallocene compounds appears to be controversial, depending on the investigated property or the measured parameter[2]. Recently we have synthesized $[\eta^5\text{-}C_5Me_4(SiMe_3)]_2TiCl_2$ and $[(\eta^5\text{-}C_5Me_4(SiMe_3)]_2TiCl$ and have found that the CE-Ti-CE (CE – centroid of the cyclopentadienyl ring) angles in these compounds are rather

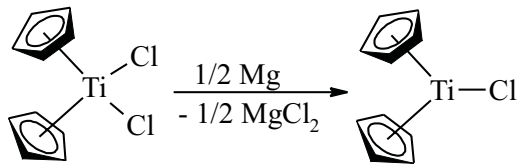

close to the corresponding angles in the permethylated compounds[3]. This is because the TMS groups are placed in side positions of the titanocene unit. Since the steric congestion in both types of compounds is close to each other, the replacement of one Me group by the TMS group should reveal the electronic effect of the latter, compared to the Me group. The ambigous behaviour of the $SiMe_3$ group has been confirmed using the above compounds. Based on the red shift of electronic absorption bands of the dichloride compared to that of $(\eta^5\text{-}C_5Me_5)_2TiCl_2$ the $SiMe_3$ group exerts a stronger electron donation effect than the Me group. On the other hand, the affinity of the monochloride to 2-methyltetrahydrofuran is close to that of the tetramethylated complex, and this would mean that the effect of the $SiMe_3$ group is close to that of hydrogen.

b) The identification of paramagnetic product in a mixture of Zr (IV), Zr (III) complexes arising as minor products in preparation of zirconocene – bis (trimethylsilyl) acetylene complexes.

The bivalent titanocene or zirconocene – bis(trimethylsilyl)acetylene complexes are thermodynamically stable but highly reactive reagents for various syntheses and also potential catalysts for linear dimerization of terminal alkynes. These compounds can be generally prepared by the reduction of metalocene dichlorides by excess magnesium in the presence of bis(trimethylsilyl)acetylene (BTMSA) in tetrahydrofuran (THF). However, the reduction of $[\eta^5\text{-}C_5Me_4(SiMe_3)]_2TiCl_2$ (**1**) under conditions which are used for preparation of methyl-substituted titanocene-BTMSA complexes gives instead of the expected $[\eta^5\text{-}C_5Me_4(SiMe_3)]_2Ti[\eta^2\text{-}C_2$

Table I
Structures of $[\eta^5\text{-}C_5H_{5-n}Me_n]_2TiCl$ compounds in toluene at –140 °C and in THF at 20 °C, and –140 °C

n	0	1	2	3	4	5
toluen, –140 C	D	D	D	M	M	M
THF, 20 °C	A	A	A	A<M	M	M
THF, –140 °C	A	A	A	A	A<M	M

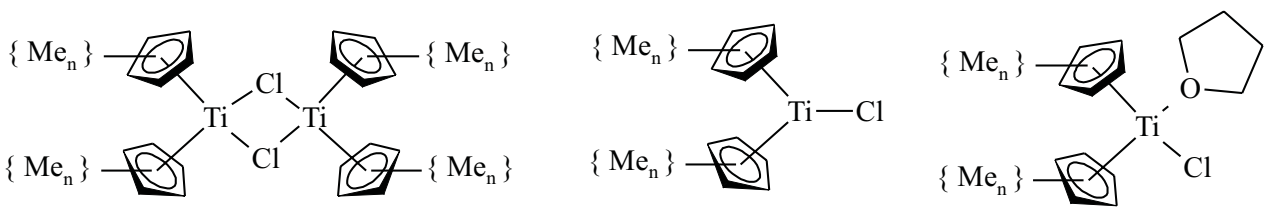

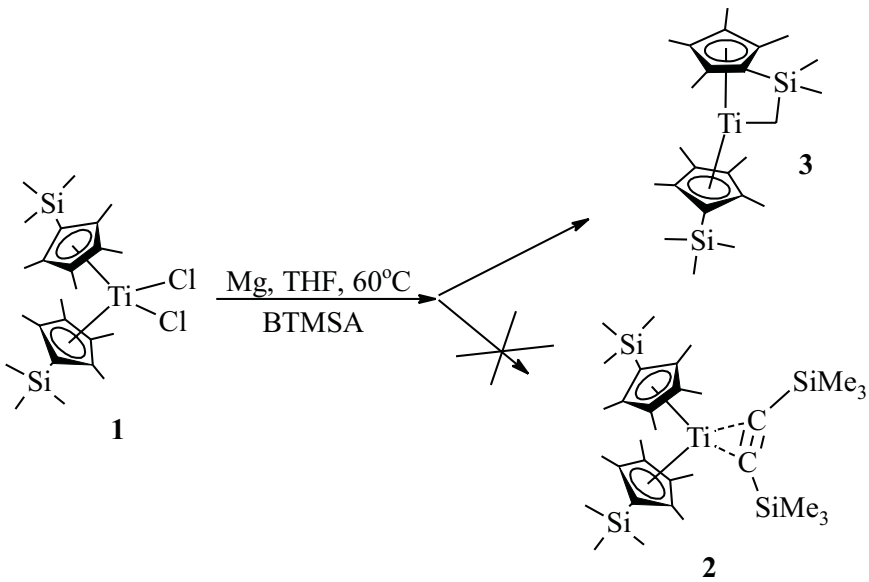

1

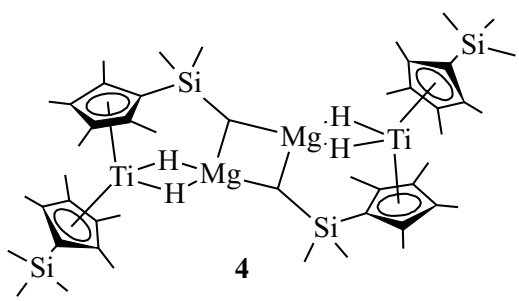

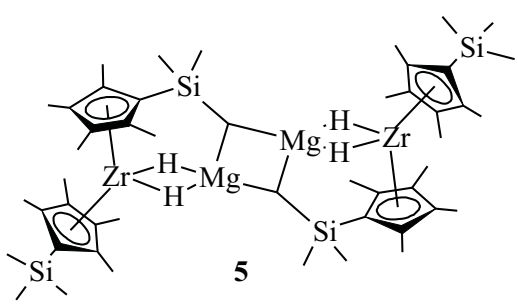

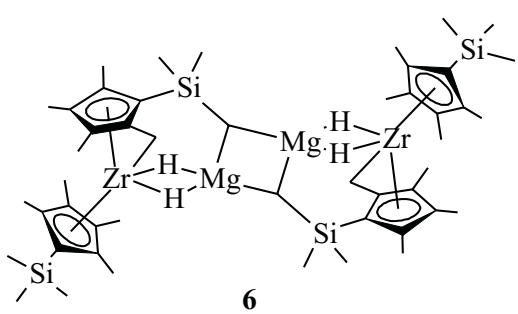

$(SiMe_3)_2$] (**2**) complex a different product. Upon heating to 60 °C in the presence of BTMSA in THF the reduction yields mainly the paramagnetic monomeric compounds (**3**) with intramolecular Si-CH_2-Ti bond (Eq. 2). This has been established by ESR spectra and by the X-ray structure. In the absence of BTMSA, the titanocene dichloride reduction affords mainly dimeric titanocene-magnesium hydride (**4**) (Chart 1). Its structure has been determined by X-ray diffraction and the presence of Ti(III) and two bridging hydrogen atoms have been proved by ESR spectra[4].

These results for titanium complexes show that the trimethylsilyl group is unexpectedly easily activated under the joint action of titanium and magnesium and that the reaction pathway depends on the presence or the absence of BTMSA. It has been therefore of interest to know how the analogous zirconocene dichloride will behave upon similar reductions.

The analogous zirconocene dichloride gives under similar conditions in the presence of BTMSA a mixture of products containing the $[\eta^5\text{-}C_5Me_4(SiMe_3)]_2Zr[\eta^2\text{-}C_2(SiMe_3)_2]$ complex as major product, and mixture of two dimeric zirconocene-magnesium hydrides as minor products[5]. These two zirconocene-magnesium hydrides have a very similar structure (Chart 1), however one contains Zr(III) (**5**) and the other Zr(IV) (**6**). We have isolated only several crystals of the tetravalent complex and have determined its crystal structure. The crystal structure has revealed that it is a centrosymetric dimer where two zirconocene-magnesium units are bound by two methylene bridges. The methylene groups are formed by abstraction of hydrogen atoms from the trimethylsilyl groups to form two two-electron three-centered Mg-C-Mg bonds. To saturate the zirconium atom, a hydrogen atom from the methyl group in the neighbourhood of the trimethylsilyl group is abstracted by the metal to produce a methylene group σ-bonded to zirconium. The both abstracted hydrogen atoms are used to build up two hydrogen bridges between the zirconium and the magnesium atoms. The second zirco-

nocene-magnesium hydride **5** could not be obtained pure by crystallization, however the ESR spectra in toluene solution and toluene glass at –140 °C of the mixture of hydrides show the triplet splitting due to a coupling of the zirconium (III) d^1 electron with two equivalent bridging hydrogen atoms. The ESR spectra of **5** (in toluene at 23 °C, g = 1.9870, a_H = 7.1 G, ΔH = 4.3 G; in toluene at –140 °C, g_1 = 2.000, g_2 = 1.989, g_3 = 1.973, g_{av} = 1.987) are similar to the spectrum of the titanocene (III)-magnesium hydride dimer **4** which has been mentioned above. This allows us to suggest that the structure of this zirconocene complex will be similar.

c) The ESR investigation of titanium-catalyzed head-to--tail dimerization of *tert*-butylacetylene.

Previously reported titanocene and zirconocene BTMSA complexes have catalyzed the linear dimerization of terminal alkynes and the catalytic cycle consists of oxidative addition and reductive elimination steps changing the valence of titanium between Ti(II) and Ti(IV)[6]. However, some Ti(III) complexes have appeared to catalyze this dimerization reaction even more effectively[7].

The catalytic system prepared by the reduction of $(\eta^5\text{-}C_5HMe_4)_2TiCl_2$ by magnesium in THF is easily followed by ESR spectroscopy since all major products are Ti(III) complexes. The reduction proceeds rapidly via the intermediate formation of blue monomeric monochloride complex $(\eta^5\text{-}C_5HMe_4)_2TiCl$ which does not coordinate THF molecule. The colour then turns to brown and the system contains mainly three products. The minor one can be easily extracted by hexane, and its structure is unknown. The products insoluble in hexane are titanocene magnesium hydride complexes. The main product is the dimeric complex $[(\eta^5\text{-}C_5HMe_4)_2Ti(\mu\text{-}H)_2Mg(THF)(\mu\text{-}Cl)]_2$ (**7**) whose ESR spectrum (Fig. 1.) does not reflect the dimeric structure. Interaction of the Ti(III) d^1 electron with two bridging hydrogen atoms (a_H = 0.7 mT) and a superhyperfine splitting with protons of the C_5HMe_4 ligands (a_H = 0.1 mT) gives three odd multiplets in the ca. 1 : 2 : 1 intensity ratio at g = 1.991. The minor product insoluble in hexane was identified by ESR measurements in glassy state. The ESR spectrum of the electronic triplet state of axial symmetry was identical with that of $[(\eta^5\text{-}C_5HMe_4)_2Ti(\mu\text{-}H)_2]_2Mg$ (**8**) (Chart 2)[8].

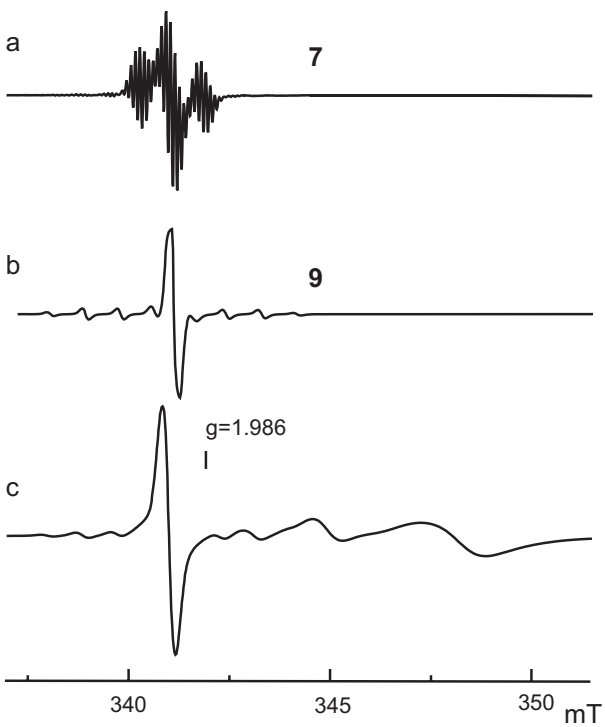

Fig. 1. **ESR spectra of the (η5-C5HMe4)2TiCl2/Mg/THF system before addition of TBUA (a) and after addition of TBUA (b)–(c). Conditions: (a) extremely diluted, measured at –15 °C, modulation amplitude 0.01 mT; (b) very diluted, at 22 °C, modulation amplitude 0.1 mT; (c) arbitrary diluted, at 22 °C, modulation amplitude 0.1 mT**

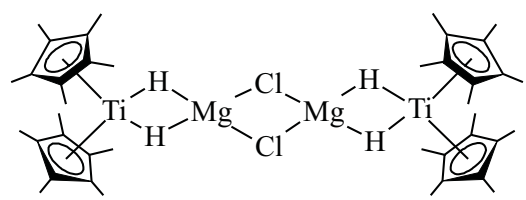

7

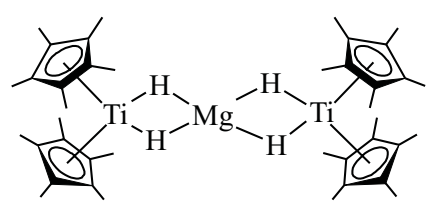

8

For the catalytic experiments, all-sealed glass devices equipped with an ESR sample tube, breakable seals and a pair of quartz cells for UV-NIR measurements have been used. After addition of tert-butylacetylene (TBUA) to $(\eta^5\text{-}C_5HMe_4)_2TiCl_2$/Mg/THF system in toluene the main component **7** is rapidly transfered into a tweezer complex $[(\eta^5\text{-}C_5HMe_4)_2Ti(\eta^1\text{-}C{\equiv}CCMe_3)_2]^-$ $[Mg(THF)(Cl)]^+$ (**9**) (Eq. 3) which is characterized by a single narrow line at g = 1.991 flanked by ca. 20 times weaker multiplets due to ^{49}Ti and ^{47}Ti isotopes (a_{Ti} = 0.85 mT). The ESR spectrum of **9** is then decreasing and new signals at g = 1.979, g = 1.968 and g = 1.951 grow in intensity. The first of them is identical with the signal of $(\eta^5\text{-}C_5HMe_4)_2TiOCMe_3$) (**10**) complex which arise from impurity in commercial TBUA. The impurity is apparently tert-butanol and the ESR spectrum of **10** as the product of deactivation is presented in all the investigated catalytic systems. The other signals are not assigned, however, they occur in all catalytically active systems.

Since compound **9** is coordinatively satutated it has only to be considered a catalytic precursor. Its dissociation affor-

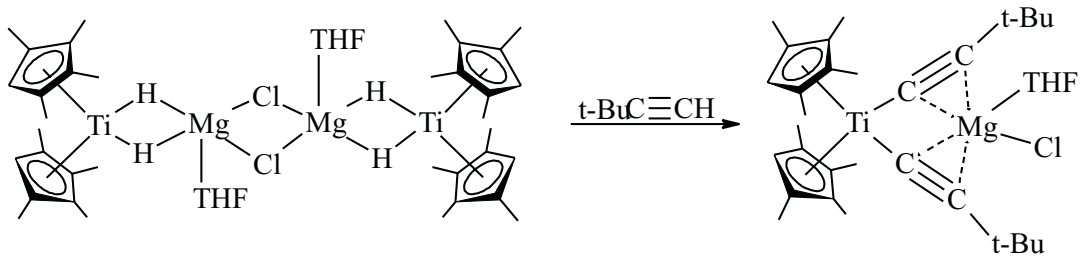

7 **9**

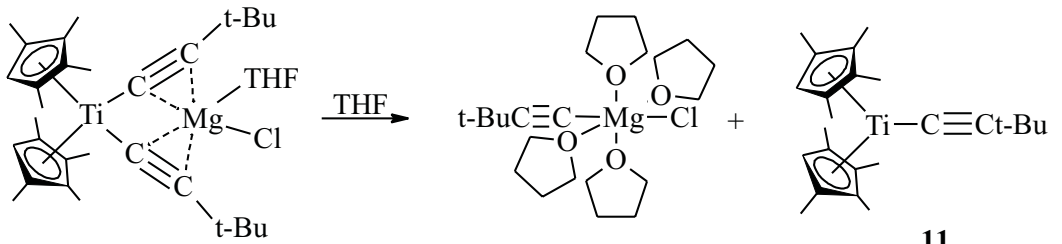

9 **11**

ding (η^5-$C_5HMe_4)_2$Ti(η^1-C≡ $CCMe_3$) (**11**), which probably displays the ESR signal B at g = 1.951 must be a subsequent inevitable step (Eq. 4). The dimerization may proceed either on the monomeric titanocene acetylide by the mechanism involving addition of TBUA to the acetylide and the elimination of the HTT dimer by hydrogen transfer by coordinating TBUA (Scheme 1).

Scheme 1 ▶

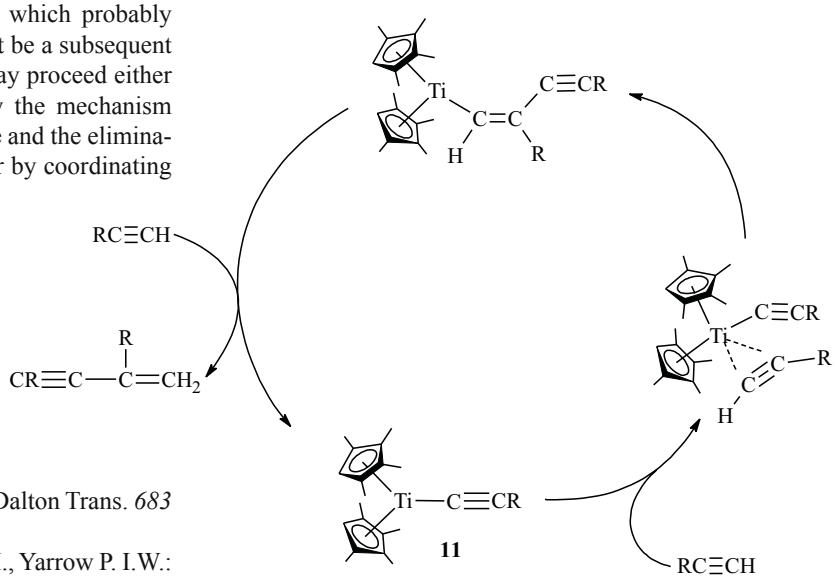

REFERENCES

1. Mach K., Raynor J. B.: J. Chem. Soc., Dalton Trans. *683* (1992).
2. a) Lappert M. F., Pickett C. J., Riley P. I., Yarrow P. I.W.: J. Chem. Soc., Dalton Trans. *805* (1981). b) Okuda J.: Topics Curr. Chem. *160*, 99 (1991). c) Gassman P. G., Deck P. A., Winter C. H., Dobbs D. A., Cao D. H.: Organometallics *11*, 959 (1992). d) Ryan M. F., Siedle A. R., Burk M. J., Richardson D. E.: Organometallics *11*, 4231 (1992). e) Finch W. C., Anslyn E. V., Grubbs R. H.: J. Am. Chem. Soc. *110*, 2406 (1988).
3. Horáček M., Gyepes R., Císařová I., Polášek M., Varga V., Mach K,: Collect. Czech. Chem. Commun. *61*, 1307 (1996).
4. Horáček M., Hiller J., Thewalt U., Polášek M., Mach K.: Organometallics *16*, 4185 (1997).
5. Horáček M., Štěpnička P., Kubišta J., Fejfarová K., Gyepes R., Mach K.: Organometallics *22*, 861 (2003).
6. a) Štěpnička P., Gyepes R., Císařová I., Horáček M., Kubišta J., Mach K.: Organometallics *18*, 4869 (1999). b) Horáček M., Štěpnička P., Kubišta J., Gyepes R., Mach K.: Organometallics *23*, 3388 (2004).
7. Horáček M., Císařová I., Čejka J., Karban J., Petrusová L., Mach K.: J. Organomet. Chem. *577*, 103 (1999).
8. Gyepes R., Mach K., Císařová I., Loub J., Hiller J., Šindelář P.: J. Organomet. Chem. *497*, 33 (1995).

L09 APPLICATIONS OF THE BENCH TOP EPR SPECTROMETER MINISCOPE MS200 IN CHEMISTRY AND LIFE SCIENCES

JOERG MUELLER
Magnettech Ltd., Volmerstrasse 9a, 12489 Berlin, Germany, j.mueller@magnettech.de

A century ago electron paramagnetic resonance (EPR) spectrometers have been large devices requiring a specialist to operate them. The bench top EPR spectrometer MiniScope MS200 is a compact, PC controlled, high performance device being easy to operate by scientists as well as by students and technical staff. The exclusive features of the MiniScope MS200 are the broad magnetic field range (0–450 mT), the big scan range (0–400 mT) and the ultra fast auto frequency control (AFC). The AFC allows stable measurements at –196 °C using a finger dewar by ultra fast control of phase changes resulting from the bubbling of the liquid nitrogen.

Samples range from liquid to solid aggregation, e. g. liquids, solutions, suspensions, blood, cells, paste, vessels, tissue, powder, solid compound. Samples can be measured at resonator temperature (32–34 °C), –196 °C using a finger dewar or between –170 and +200 °C using our Temperature Controller TC H02.

Beside research application the MiniScope MS200 can also be used for routine measurements using one of our options for automatic or semiautomatic measurements.

The main applications in life sciences are the detection and quantification of nitric oxide (NO) and oxygen centred radicals like superoxide anions and hydroxyl radicals in cells, tissue, vessels and biological fluids.

In food chemistry EPR is used to measure the antioxidative features of foodstuff. In petrol chemistry radicals serve as polymerization inhibitors during distillation of unsaturated hydrocarbons. In bioinorganic chemistry the environment of transition metal centres can be compared with that of low molecular weight complexes designed to mimic the enzyme function.

This selection of applications demonstrates that the MiniScope MS200 is of great benefit for a variety of sciences because it can be applied universally.

L10 PHOTOINDUCED GENERATION OF REACTIVE INTERMEDIATES IN TITANIUM DIOXIDE SUSPENSIONS INVESTIGATED BY EPR SPIN TRAPPING TECHNIQUE: N-OXIDE VS. NITRONE SPIN TRAPPING AGENTS

DANA DVORANOVÁ, VLASTA BREZOVÁ and HELENA ŠVAJDLENKOVÁ
Department of Physical Chemistry, Faculty of Chemical and Food Technology, Slovak University of Technology in Bratislava, Radlinského 9, SK-812 37, Slovak Republic, dana.dvoranova@stuba.sk

Introduction

The efficient photocatalytic remediation of pollutants from aqueous environment requires the formation of reactive radical species suitable for the non-selective oxidations of pollutants[1–5]. EPR spin trapping technique represents crucial method for radical identification and relative quantification. The irradiation of TiO_2 powder in oxygenated aqueous media resulted in the generation of reactive radical species (mainly ROS – *reactive oxygen species,* e. g. $^{\bullet}OH$, $^{\bullet}OOH/O_2^{\bullet-}$, H_2O_2, $^1O_2$). Upon ultra-band gap irradiation of TiO_2 particles positive holes (h^+) are generated in the valence band and negative electrons (e^-) appear in the conduction band of a TiO_2 semiconductor as in Eq. 1 (ref.[3,5,6])

$$TiO_2 + h\nu \rightarrow TiO_2(e^- + h^+) \quad (1)$$

The photogenerated charge carriers may be involved in redox processes at the TiO_2 surface. Positive holes are trapped by surface hydroxyl groups forming reactive hydroxyl radicals in aquatic media Eq. 2

$$OH^- + h^+ \rightarrow {}^{\bullet}OH \quad (2)$$

In aerated systems oxygen serves as a very effective electron acceptor producing super oxide anion radicals, according to Eq. 3

$$O_2 + e^- \rightarrow O_2^{\bullet-} \quad (3)$$

In the aqueous TiO_2 suspensions super oxide radical anions may act as oxidizing agents or as an additional source of hydroxyl radicals via the subsequent formation of hydrogen peroxide as in Eqs. 4–7

$$O_2^{\bullet-} + H^+ \rightarrow {}^{\bullet}OOH \quad (4)$$
$$2\ {}^{\bullet}OOH \rightarrow H_2O_2 + O_2 \quad (5)$$
$$H_2O_2 + O_2^{\bullet-} \rightarrow {}^{\bullet}OH + O_2 + OH^- \quad (6)$$
$$H_2O_2 + h\nu \rightarrow 2\ {}^{\bullet}OH \quad (7)$$

The photoproduced short-lived reactive radical intermediates, generally marked $^{\bullet}R$, may be trapped by diamagnetic spin trapping agents, forming more stable paramagnetic ad-

ducts. The nature of the radical added can be identified after the analysis and simulation of the experimental EPR spectra.

The commonly used spin trapping agents in photochemical systems are nitrone and N-oxide derivatives[7]. The nitrone and N-oxide spin traps react with free radical species via a carbon located in a β-position relative to the nitrogen. An important feature of spin trapping agents is their stability in photochemical systems.

Our investigations were focused on the comparison of N-oxide and nitrone spin trapping agents photostability and reactivity, using 5,5-dimethyl-1-pyrroline N-oxide (DMPO), 3,3,5,5-tetramethyl-1-pyrroline N-oxide (TMPO), α-(4-pyridyl-1-oxide)-N-*tert*-butylnitrone (POBN) and 4-(N--methyl-pyridyl)-N-*tert*-butylnitrone (MePyPB) in the TiO_2 photocatalytic systems.

Experimental

Titanium dioxide (Degussa P25, specific area of 50 m^2 g^{-1}) was applied in photocatalytic experiments. Table I summarizes names and abbreviations of used spin trapping agents (Aldrich) and stable free radical (Aldrich). The stock suspensions of TiO_2 were prepared in redistilled water and TiO_2 slurry was mixed with aqueous solutions of spin trap or spin label prior to irradiation. The prepared suspensions were saturated by oxygen, filled in the quartz flat cell optimized for the Bruker TM cylindrical EPR cavity. The X-band EPR spectra were recorded at EPR Bruker EMX spectrometer equipped with a TM-110 (ER 4103 TM) cylindrical cavity. The samples were irradiated directly in the cavity of EPR spectrometer by HPA 400/30S medium-pressure lamp (Philips), and the EPR spectra were measured in situ. The lamp irradiance in UV/A region of 30 mW cm^{-2} inside the EPR cavity was evaluated by a Compact radiometer UVPS (UV Process Supply, Inc. USA). The radiation with wavelengths $\lambda > 300$ nm was selected by a Pyrex filter. The standard EPR experiments were performed at 293 K. The simulations of the individual components in the complex EPR spectra were obtained using WinEPR and SimFonia programs (Bruker).

Table I
Names, abbreviations and structures of used spin trapping agents and stable free radical TEMPOL

Abbreviation, name	Structure
DMPO 5,5-dimethyl-1-pyrroline-N-oxide	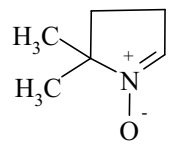
TMPO 3,3,5,5-tetramethyl-1-pyrroline-N-oxide	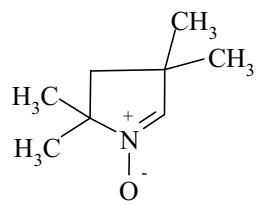
POBN α-(4-pyridyl-1-oxide)-N-*tert*-butylnitrone	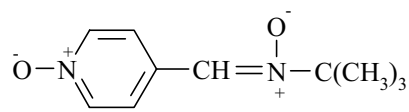
MePYBN 4-(N-methylpyridyl)-N-*tert*-butylnitrone	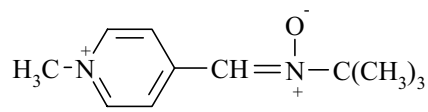
TEMPOL 4-hydroxy-2,2,6,6-tetramethyl-4-piperidine N-oxyl	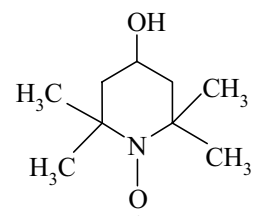

The experimental EPR spectra were fitted as the linear combinations of these individual simulations using a least--squares minimization procedure with the Scientist Program (MicroMath).

Results and discussion

DMPO is widely used spin trapping agent in the study of oxygen-centered free radicals, due to its solubility in water and the formation of more stable nitroxide adducts. DMPO reacts with hydroxyl radical forming •DMPO-OH adduct according to Eq. 8.

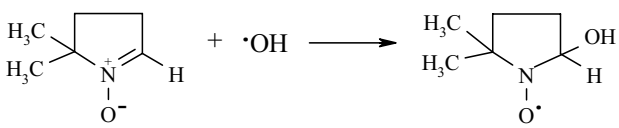

DMPO + ·OH → ·DMPO-OH (8)

For •DMPO-OH paramagnetic adduct generated in TiO_2 aqueous suspensions is typical four-line EPR signal, which is characterized with spin Hamiltonian parameters $a_N = a_H = 1.49$ mT and $g = 2.0057$. Fig. 1. represents experimental and simulated EPR spectra of obtained upon 60 s *(a)* and 600 s *(b)* of continuous irradiation of oxygen-saturated aqueous TiO_2 suspension in the presence of DMPO. In oxygen-saturated aqueous TiO_2 suspensions the increase of •DMPO-OH adduct is very fast, maximal relative intensity of the EPR signal was observed after 40 s of irradiation. Upon prolonged exposure the EPR relative intensity of •DMPO-OH adduct decreased. According to the literature, the half-life of the •DMPO-OH adduct in an aqueous environment is about 15 min[7]. The fast decrease of the EPR relative intensity of •DMPO-OH monitored upon continuous irradiation can be rationalized by assuming multiple additions of hydroxyl radicals to DMPO or its oxidation by holes forming EPR silent products or the fast consumption of oxygen in the experimental system (EPR flat cell), lowering so the effective charge carrier separation and hydroxyl radical formation. Upon prolonged exposure of system with higher concentration of TiO_2 (over 0.25 mg ml^{-1}) a new paramagnetic signal is observed, which is attributed to the •DMPO-X adduct with characteristic hyperfine splitting constants $a_N = 0.730$ mT, $a_H(2H) = 0.390$ mT and significantly higher $g = 2.0065$. This adduct is formed as product of spin trap oxidation either by multiple addition of hydroxyl radical to the DMPO pyrroline skelet or oxidation by singlet oxygen[8,9].

It should be noted here, that another reaction pathway of generation •DMPO-OH adducts in the irradiated TiO_2 suspensions is also possible; •DMPO-OH could be the generated as hydrolysis product of $DMPO^{\bullet+}$ cation radical formed by hole oxidation in accordance with Eqs. 9–10 (ref.[10])

$$DMPO + h^+ \rightarrow DMPO^{\bullet+} \quad (9)$$

$$DMPO^{\bullet+} + H_2O \rightarrow {}^{\bullet}DMPO\text{-}OH + H^+ \quad (10)$$

Fig. 1. also shows experimental and simulated EPR spectra obtained upon 60 s *(a)* and 600 s *(b)* of continuous irradiation of oxygen-saturated aqueous TiO_2 suspension in the presence of TMPO, tetramethyl-substituted analogue of pyrroline N-oxide spin trapping agent. Upon 60 s exposure time, the •TMPO-OH paramagnetic adduct is observed, characterized by hyperfine splitting constants with $a_N = 1.531$ mT, $a_H = 1.68$ mT and $g = 2.0057$, which is attributed to the addition of hydroxyl radical to TMPO and carbon-centered signal •TMPO-CR ($a_N = 1.597$ mT, $a_H = 2.44$ mT and $g = 2.0056$) originated from photochemical degradation of TMPO molecule. After prolonged irradiation in the presence of higher concentration of TiO_2 in system, another signal is observed. This adduct is assigned to the product of oxidation of TMPO molecule to •TMPO-X ($a_N = 0.69$ mT and increased $g = 2.0062$), which is more stable than •DMPO-X, and reflects well the concentration of TiO_2 in irradiated system.

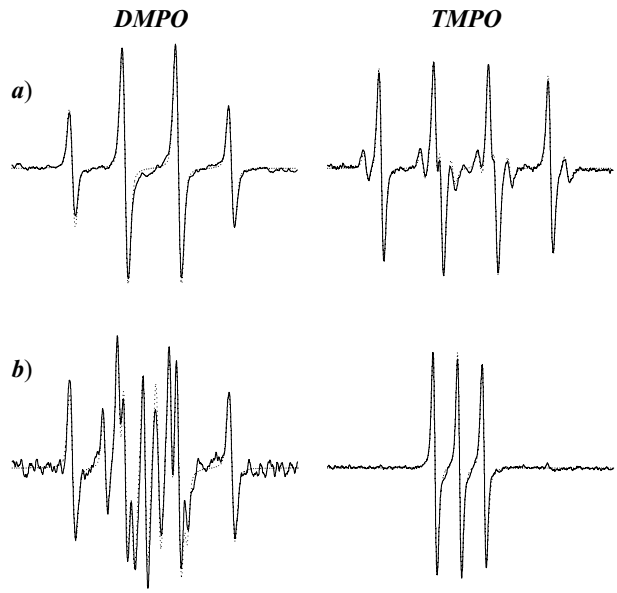

Fig. 1. **Experimental (solid line) and simulated (dotted line) EPR spectra (sweep width 8 mT) obtained upon** a) **60 s and** b) **600 s continuous irradiation of oxygen-saturated TiO_2 aqueous suspensions in the presence of DMPO and TMPO spin trapping agents; $c_{spin\ trap} = 0.01$ mol dm^{-3}; $c(TiO_2) = 0.571$ mg ml^{-1}**

Fig. 2. represents the experimental and simulated EPR spectra obtained upon 600 s continuous irradiation of oxygen-saturated TiO_2 aqueous suspension in the presence of POBN and MePYBN spin trapping agents belonging to the group of tert-butyl nitrone derivatives. However, these spin trapping agents revealed only small selectivity of the hyperfine splitting constants on the character of the free radical added. Upon prolonged exposure in both systems only one type of paramagnetic adduct was observed. This signal was attributed to the addition of hydroxyl radical to spin trap molecule; i. e., in the presence of POBN as •POBN-OH with

hyperfine splitting constants $a_N = 1.477$ mT, $a_H = 0.142$ mT and $g = 2.0057$ and, •MePYBN-OH ($a_N = 1.499$ mT, $a_H = 0.163$ mT and $g = 2.0057$) in the presence of MePYBN, respectively. Both signals reflected the good stability of generated spin adducts in the reaction systems and no another signal was observed under given experimental conditions.

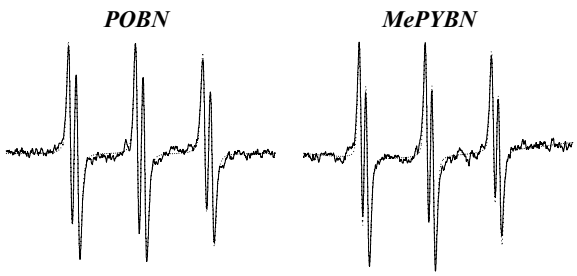

Fig. 2. **Experimental (solid line) and simulated (dotted line) EPR spectra (sweep width 6 mT) obtained after 600 s continuous irradiation of oxygen-saturated TiO_2 aqueous suspensions in the presence of POBN and MePyBN spin trapping agents; $c_{spin\ trap} = 0.01$ mol dm^{-3}; $c(TiO_2) = 0.571$ mg ml^{-1}**

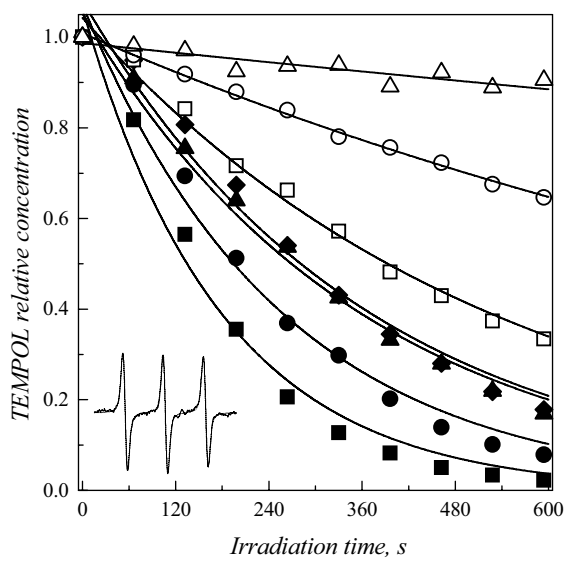

Fig. 3. **The dependence of TEMPOL relative concentration on irradiation time determined in the oxygen-saturated TiO_2 aqueous suspensions. The concentration of TiO_2 (mg ml^{-1}): △ 0; ○ 0.095; □ 0.19; ◆ 0.286; ▲ 0.391; ● 0.476; ■ 0.571. Initial concentration of TEMPOL was $c_{TEMPOL} = 2.3$ μmol dm^{-3}. Inset represents experimental (solid line) and simulated (doted line) EPR spectra (sweep width 6 mT) of TEMPOL obtained before continuous irradiation in the oxygen-saturated TiO_2 aqueous suspensions with spin Hamiltonians parameters $a_N = 1.70$ mT and $g = 2.0060$**

The application of photochemically stable free radical TEMPOL for the detection of free radical formation (monitoring as the decrease of its EPR intensity resulting from the interaction of its >N-O• group with the generated reactive radical species[11]) showed the substantial decrease of reactive radical species in oxygen-saturated TiO_2 aqueous suspensions (Fig. 3.). The decline of EPR relative intensity is caused mainly by reaction of hydroxyl radicals with TEMPOL and is proportional to the concentration of TiO_2 in chemical system. The concurrent reaction with singlet oxygen or direct reduction of TEMPOL by photogenerated electron cannot be excluded.

Conclusion

The application of DMPO and TMPO as the spin traps confirmed the presence of hydroxyl radical adducts. The prolonged irradiation of photocatalytic systems with TiO_2 concentration over 0.25 mg ml^{-1} caused the oxidative decomposition of N-oxide spin traps via radical intermediates under given experimental conditions. The nitrone spin traps POBN and MePyBN shown high stability upon irradiation, and the relative concentration of radical adducts increased with TiO_2 amount in the irradiated suspensions. The generation of reactive radical intermediates was shown using stable nitroxide radical TEMPOL monitoring the decline of its EPR signal intensity during exposure.

We thank Slovak Grant Agency for the financial support (Project VEGA/1/0053/03).

REFERENCES

1. Li A. S. W., Cummings K. B., Fujishima H. A. et al.: J. Photochem. Photobiol. C: Photochem. Rev. *1*, 1 (2000).
2. Alfano O. M., Bahnemann D. W., Cassano A. E. et al.: Catalysis Today *58*, 199 (2000).
3. Hoffmann M. R., Martin S. T., Choi W., Bahneman D. W.: Chem. Rev. *95*, 69 (1995).
4. Fox M. A., Dulay M. T.: Chem. Rev. *93*, 341 (1993).
5. Brezová V., Staško A., Biskupič S. et al.: J. Phys. Chem. *98*, 8977 (1994).
6. Dvoranová D., Brezová V., Mazúr M. et al.: Appl. Catal. B: Environ. *37*, 91 (2002).
7. Roethling P., Buettner G. R., Chignell C. F.: J. Magn. Reson. *79*, 140 (1988).
8. Konaka R., Kasahara E., Dunlap W. C. et al.: Free Radic. Biol. Chem. *27*, 294 (1999).
9. Bilski P., Reszka K., Bilska M., Chignell C. F.: J. Am. Chem. Soc. *118*, 1330 (1996).
10. Eberson L., MacCullough J. J., Persson O.: J. Chem. Soc. Perkin Trans *2*, 133 (1997).
11. Brezová V., Gabčová S., Dvoranová D., Staško A.: J. Photochem. Photobiol. B: Biol. in press (2005).

L11 QUANTITATIVE EPR SPECTROSCOPY – A RELIABLE AND REPRODUCIBLE ANALYTICAL TECHNIQUE

MILAN MAZUR[a], JAN MONCOL[b] and MARIAN VALKO[a]
[a]*Department of Physical Chemistry,*
[b]*Department of Inorganic Chemistry, Faculty of Chemical and Food Technology, Slovak University of Technology, Radlinského 9, SK-812 37 Bratislava, Slovak Republic; milan.mazur@stuba.sk*

Introduction

EPR spectroscopy is a very useful analytical technique for the detection of paramagnetic species in chemical, physical and biological systems. One of the most important aspects of EPR is to determine the concentration of radical species, particularly in biological systems. The aim of this contribution is to provide a short overview of quantitative analysis of samples containing radical species by means of quantitative EPR spectroscopy.

As pointed out by Prof. J. S. Hyde[1] over forty years ago: "of all the measurements one can make with EPR equipment, the determination of spin concentration is the most difficult". This fact was fully confirmed in the results obtained from the international experiments carried out in 1962 (coordinated by Prof. W. Kohnlein[2]) and 1991–1992 (coordinated by Prof. N. D. Yordanov[3]), which results clearly demonstrated the essential difficulties in quantitative EPR spectroscopy.

Error sources in quantitative EPR measurement

A multitude of sources of error influences the accuracy and reproducibility of quantitative EPR spectroscopy (see elsewhere,[1–25]). The error sources can be divided into two main groups: (i) primary error sources (including sample- and instrumental- associated factors) and (ii) secondary error sources (including data processing-, EPR standards- and calibration- associated problems, and human- associated factors). The list of instrumental and sample associated variables, which can affect quantitative EPR measurements, is very extensive[6], and the majority of these errors occur simultaneously and synergistically.

The essential problem is that some of these above-mentioned sources of error may cause significant systematic and/or non-systematic errors in quantitative EPR measurements. The majority of such error sources can be controlled by the EPR spectrometer operator; however, certain sample-associated errors can be partially influenced, or controlled directly by the quantitative measurement applicants, who are only EPR spectroscopy users, not the EPR spectroscopy specialists/operators. These errors mainly involve sample shape, in the case of bulk solid-state materials, and sample packing procedure, in the case of solid-state powder or polycrystalline materials.

The most effective way to minimise the influence of such error sources in quantitative EPR spectroscopy would be to use the same standardised procedures for all EPR measurements and post-recording spectral manipulations. However, the crucial problem in obtaining improved accuracy and reproducibility lies in maximising the quality of the input data and not in the subsequent computational procedures. For example, double integration of EPR spectra can be accomplished with a precision of 2 % or better, when a computer-interfaced spectrometer (required for quantitative measurements) is used[9].

As has been clearly shown in the literature [5,6,10–23], the most important primary error sources in quantitative EPR measurements are as follows: i) sample-associated factors (see Table I for more details) including variation of the sample material (dielectric constant), sample size and shape, sample tube wall thickness, and sample orientation and positioning within the microwave cavity, and ii) instrument-

Table I
A list of the most challenging sample-related factors. Primary error sources in quantitative EPR measurements, which are associated with sample preparation, sample containers, and sample insertion into the microwave cavity.

SAMPLE-ASSOCIATED FACTORS			
Sample preparation		Sample containers	
Sample material	Dielectric constant	Cylindrical sample tube	Flat-cell sample
– liquid – solid (monocrystal or powder)	– loss solvent sample – high dielectric loss materials with hight conductivity	– wall thickness of quartz cylindrical tube and flat cell – "sucking-in" and "lens effect"	
Sample volume and shape – sample shape vs. sample volume		*Sample insertion into the cavity* – sample positioning and orientation	
Packing problem – packing density for powder and polycrystalliene materials		– sample alignment procedure	

-associated factors (see Table II for further details) including variation of the EPR spectrometer set-up parameters, cavity Q-factor, spectrometer sensitivity, and the presence/absence of a variable-temperature quartz Dewar during the measurement. Variation in these parameters could cause significant errors in the primary phase of quantitative EPR analysis (i. e., data acquisition). Therefore, the above-mentioned topics were recently systematically studied in our EPR laboratory[10–16,24,25].

Table II
A list of the most challenging instrument-relassociated factors. Primary error sources in quantitative EPR measurements, which are associated with the microwave cavity, EPR spectrometer parameters, and variable-temperature quartz Dewars

INSTRUMENT-ASSOCIATED FACTORS	
Microwave cavity	Modulation frequency
– microwave field profile	– modulation field profile
– power intensity (saturation)	– modulation coil location
– cavity Q-factor	– modulation coil diameter
– filling factor	**Variable-temperature quartz Dewar**
– spectrometer sensitivity	– presence/absence during measurement
– single or double cavity	– wall thickness of quartz Dewar
– cavity for flat-cell geometry	– "sucking-in" and "lens effect"

The main aim of this contribution is to give useful tips, suggestions, recommendations, and simple procedures to minimise the influence of the above-selected primary error sources in quantitative EPR measurements. We believe that the tips outlined in the next section of this report would be helpful in quantitative EPR practice.

Catalogue of useful tips, suggestions and recommendations

According to literature data[1–9,17–23], as well as results obtained in our EPR laboratory [10–16,24,25], the following are recommendations for samples that are to be compared in quantitative EPR studies.

S i n g l e o r d o u b l e m i c r o w a v e c a v i t y

A double TE_{104} rectangular cavity should be used in quantitative EPR spectroscopy. (Unknown and standard samples are measured simultaneously with the same instrument setting).

D i e l e c t r i c c o n s t a n t o f s a m p l e m a t e r i a l

Dielectric properties of unknown and standard samples should be as close as possible. (An apparent increase of signal intensity due to the "field compression effect" in double cavity occurs when the unknown has a higher dielectric constant than the standard).

S a m p l e s h a p e v e r s u s s a m p l e v o l u m e

All samples to be compared in quantitative EPR spectroscopy should have identical shape. (Identical volume, or identical sample weight, are insufficient criteria).

S a m p l e p a c k i n g p r o c e d u r e

The packing density and volume weight of the unknown and reference powder samples should be as nearly identical as possible. (A special procedure for sample packing from powder material should be used).

S a m p l e p o s i t i o n i n g i n t h e c a v i t y

Accurate and precise positioning of each sample in the microwave cavity is the principal, necessary, and imperative condition in quantitative EPR spectroscopy. (In the ideal case, the sample centre coincides with the centre of the cavity).

T i p o f s a m p l e a l i g n m e n t p r o c e d u r e

A special alignment procedure for the accurate and precise positioning of samples in the microwave cavity is essential in quantitative EPR spectroscopy. (The sample position in the cavity at which the signal intensity is a maximum should be specified).

C y l i n d r i c a l s a m p l e c o n t a i n e r s a n d q u a r t z D e w a r s

All cylindrical samples to be compared in quantitative EPR analysis should have an identical wall thickness of sample tubes. Regardless of sample type, every EPR spectrum must be recorded inside the identical variable-temperature quartz Dewar, if used. (An apparent increase of signal intensity occurs when the unknown tube walls are thicker than the standard and/or a quartz Dewar is used for the unknown – the "lens effect").

P l a n a r s a m p l e g e o m e t r y

Planar samples to be compared in quantitative EPR should have identical length and width, and must be identically centred and angularly positioned within the microwave cavity. (Maximum signal intensity is usually obtained for a planar sample when the sample plane is parallel to the wave guide in the cavity).

" O v e r f u l l - l e n g t h c a v i t y " s a m p l e

When "over full-length cavity" (i. e., sample extends outside cavity) cylindrical and planar samples are to be compared in quantitative EPR the unknown and standard should have identical length and must be identically positioned in the microwave cavity. The length of "over full-length cavity" samples should be less than double the cavity length. (Existence of "sloping plateau" region with additional oscillating signal superimposed).

T i p o f s a m p l e g e o m e t r y

A capillary of length 30 mm with i. d. less than 1.5 mm can be a suitable type of sample geometry for quantitative

analysis of both low and high dielectric loss materials in the X-band double TE_{104} rectangular cavity. (Such a sample holdershape provides a suitable compromise of minimising field perturbations and maximising signal/noise ratio).

Concluding remarks

When the above-mentioned tips, recommendations and procedures were used in our quantitative EPR experiments (~~using~~ a field modulated CW Bruker ER 200 D-SRC with Aspect computer EPR spectrometer with the original Bruker double TE_{104} (ER 4105 DR) rectangular cavity; constant laboratory temperature maintained by air conditioning) the EPR signal intensity of a wide range of samples could be obtained with the experimental error in the range 2–5 %. However, if these special precautions were not employed, then error~~s~~ could be in excess of 20 %.

The results of systematic investigations as well as the author's own experience suggest that quantitative EPR spectroscopy will be in the new millennium a reliable and reproducible analytical technique and no longer a source only of inaccuracies, errors and artefacts.

This work was supported by Science and Technology Assistance Agency under the contact No. APVT-20-005702, and by Slovak Grant Agency for Science (VEGA 1/2450/05 and VEGA 1/0053/03). The author is grateful to Dr. H. Morris for fruitful discussions during the course of this work.

REFERENCES

1. Hyde J. S.: *Experimental Techniques* in EPR, Proceedings of the 6th Annual NMR-EPR Workshop, Varian Association Instrument Division, Palo Alto, California, 1962.
2. Kohnlein W.: *Radiation Effects in Physics, Chemistry and Biology,* (Ebert M., Howard A., eds.), p. 206, Nortd-Holland, Amsterdam, 1963.
3. Yordanov N. D., Ivanova M.: Appl. Magn. Reson. *6*, 333 (1994).
4. Blanchard S. C., Chasteen N. D.: Anal. Chim. Acta *82*, 113 (1967).
5. Casteleijn G., ten Bosch J. J., Smidt J.: Appl. Phys. *39*, 4375 (1968).
6. Warren D. C., Fitzgerald J. M.: Anal. Chem. *49*, 250 (1977).
7. Goldberg I. B., Crowe, H. R., Robertson W. M.: Anal. Chem. *49*, 962 (1977).
8. Goldberg I. B.: J. Magn. Reson. *32*, 233 (1978).
9. Burns D. T., Flockhart B. D.: Phil. Trans. R. Soc. London A 333, 37 (1990).
10. Mazúr M., Valko M., Morris H., Klement R.: Anal. Chim. Acta *333*, 253 (1996).
11. Mazúr M., Morris H., Valko M.: J. Magn. Reson. *129*, 188 (1997).
12. Mazúr M., Morris H., Valko M.: J. Magn. Reson. *42*, 37 (2000).
13. Mazúr M., Valko M., Morris H.: Appl. Magn. Reson *20*, 317 (2001).
14. Mazúr M., Valko M., Morris H.: Anal. Chim. Acta *443*, 127 (2001).
15. Mazúr M., M. Valko, H. Morris: Anal. Chim. Acta *482*, 229 (2003).
16. Mazúr M., Moncol J., Valko M., Morris H.: Anal. Chim. Acta *526*, 163 (2004).
17. Rataiczak R. D., Jones M. T.: J. Chem. Phys. *56*, 3898 (1969).
18. Kooser R. G., Volland W. V., Freed J. H.: J. Chem. Phys. *50*, 5243 (1969).
19. Goldberg I. B., Schneider G. R.: J. Chem. Phys. *65*, 147 (1976).
20. Dalal D. P., Eaton S. S., Eaton G. R.: J. Magn. Reson. *44*, 415 (1981).
21. Barklie R. C., Sealy L.: J. Magn. Reson. *97*, 611 (1992).
22. Nagy V. J., Plaček J.: Fresenius' J. Anal. Chem. *343*, 863 (1992).
23. Nagy V.: Appl. Magn. Reson. *6*, 256 (1994).
24. Mazúr M., Valko M., Klement R., Morris H.: Anal. Chim. Acta *333*, 249 (1996).
25. Mazúr M., Valko M., Morris H.: Rev. Sci. Instrum. *68*, 2514 (1997).